

We are IntechOpen, the world's leading publisher of Open Access books Built by scientists, for scientists

6,900

Open access books available

186,000

International authors and editors

200M

Downloads

Our authors are among the

154

Countries delivered to

TOP 1%

most cited scientists

12.2%

Contributors from top 500 universities



WEB OF SCIENCE™

Selection of our books indexed in the Book Citation Index
in Web of Science™ Core Collection (BKCI)

Interested in publishing with us?
Contact book.department@intechopen.com

Numbers displayed above are based on latest data collected.
For more information visit www.intechopen.com



Diagnosis of Electrochemical Impedance Spectroscopy in Lithium-Ion Batteries

Quan-Chao Zhuang¹, Xiang-Yun Qiu^{1,2}, Shou-Dong Xu^{1,2},
Ying-Huai Qiang¹ and Shi-Gang Sun³

¹*Li-ion Batteries Lab, School of Materials Science and Engineering,*

²*School of Chemical Engineering and Technology,*

China University of Mining and Technology, Xuzhou

³*State Key Laboratory of Physical Chemistry of Solid Surfaces,*

Department of Chemistry, College of Chemistry and Chemical Engineering,

Xiamen University, Xiamen,

China

1. Introduction

The establishment of Electrochemical Impedance Spectroscopy (EIS), sometimes called AC impedance spectroscopy, has been initiated from 1880 to about 1900 through the extraordinary work of Oliver Heaviside. The EIS has been developed basically in the field of wet electrochemistry. In particular, the names of Sluyters, Sluyters-Rehbach[90, 91] (as well as many others) are strongly linked to this research field. Nowadays, there are no doubts that EIS has become a powerful tool for the analysis of complex processes (such as corrosion) that are influenced by many variables with regard to electrolyte, materials and interfacial geometry. The power of the technique arises from[55]: (i) it is a linear technique and hence the results are readily interpreted in terms of Linear Systems Theory; (ii) if the measurements are over an infinite frequency range, the impedance (or admittance) contains all of the information that can be gleaned from the system by linear electrical perturbation/response techniques; (iii) the experimental efficiency (amount of information transferred to the observer compared to the amount produced by the experiment) is particularly high; (iv) the validity of the data is readily determined using integral transform techniques (the Kramers–Kronig transforms) which are independent of the physical processes involved.

EIS data are often interpreted by using electrical equivalent circuits (EECs). However, the EECs are merely analogs, rather than models. But we use the EECs as a model to describe an electrochemical reaction that takes place at the electrode/electrolyte interface. Therefore they must be used with great care. The priority is to examine whether or not an EEC can indeed be appropriate as a model for the reaction at the electrified interface. It is worthwhile noting that the ultimate goal of using EIS is to characterize the mechanism of the charge transfer reaction, and thus the mere development of an analog (which is now done by various computer programs) represents an incomplete analysis of the data. For the parametric identification, the complex nonlinear least-squares (CNLS) method is used. The method is based on fitting object model parameters to the impedance spectrum[60].

In the past decades, EIS has been extensively used in the analysis of lithium battery systems, especially to predict the behavior of batteries, and to determine the factors limiting the performance of an electrode including its conductivity[75, 126], charge-transfer properties[11, 103, 117-119], properties of the passivating layer, etc. Numerous recent studies have been published on various aspects of the insertion electrodes used in lithium-ion batteries for the attempt to understand the origin of the observed capacity loss during extended cell cycling or storage[1, 30, 37, 52, 66, 78, 97].

EIS is now described in the general books on electrochemistry[9, 18, 27, 33, 56, 107], specific books[13, 59, 77] on EIS, and also by numerous articles and reviews[17, 22, 41-43, 55, 57, 87]. It became very popular in the research and applied chemistry. If a novice to EIS interested in the subject matter of this fundamental review, he/she may be strongly recommend to read the superb EIS text by Macdonald[13, 59] and Orazem et al.[77], along with a compilation of excellent research articles[24, 58, 60, 79, 121], in order to obtain a good grounding in the fundamental principles underpinning the EIS technique, as this rudimentary information is beyond the scope of this specialized review paper. The purpose of this chapter is to review recent advances and applications of EIS in the development of the kinetic model for the lithium insertion/extraction into intercalation materials and the lithiation/delithiation of simple binary transition metal compounds which can achieve reversible lithium storage through a heterogeneous conversion reaction. The typical impedance spectra and the ascription of each time constant of EIS spectra are discussed based on analyzing the potential and temperature dependence of the common EIS features. The potential and temperature dependence of the kinetic parameters, such as the charge transfer resistance, the electronic resistance of activated material, the resistance of lithium ions transferring through SEI film, the Schottky contact resistance, are also discussed based on the theoretical analysis. Moreover, the influences of non-homogeneous, multilayered porous microstructure of the intercalation electrode on the EIS feature and the kinetic parameters are discussed based on the experimental results and theoretical analysis. Finally, the inductance formation mechanism is reviewed.

2. Kinetic models for lithium ions insertion into the intercalation electrode

The intercalation electrode reaction[100, 111]:



is a special redox reaction, in which A^+ is the cation (e.g. Li^+ , H^+ , etc.) in the electrolyte, $\langle H \rangle$ represents the host molecule (e.g. TiS_2 , WO_3 , etc.), $A_x \langle H \rangle^{x-}$ is the nonstoichiometric intercalate produced. The reactions are characterized by the reversible insertion of guest species into a host lattice without significant structural modification of the host in the course of intercalation and deintercalation. The intercalation reactions are widely used in lithium-ion batteries and in the electrochemical synthesis of intercalates.

It can be seen that the electrode composition changes during an intercalation electrode reaction, which is different from the usual first kind metal electrode reaction occurring only by electron transfer at electrode/electrolyte interfaces. The sequence of transport processes of the cations involves lithium ions transport process, the electron transport process, and the charge transfer process. Due to the differences in their time constants, EIS is a suitable technique to investigate these reactions and can allow us to separate most of these

phenomena. Therefore, using EIS to analyze the kinetic parameters related to lithium ions insertion/extraction process in intercalation materials such as the SEI film resistance, charge transfer resistance, as well as the relationship between the kinetic parameters and the potential or temperature, is helpful to understand the reaction mechanism of lithium ions insert into (extract from) the intercalation materials, to study degradation effects, to facilitate further electrode optimization, and to improve the charge/discharge cycle performance as well as the rate capability of lithium-ion batteries. A major problem of impedance spectroscopy as an electroanalytical tool is the fact that, in most cases, impedance spectra cannot be simulated unambiguously by a single model. Hence, major efforts are invested by prominent electrochemical groups in the development of reliable and comprehensive models that can precisely and logically explain the impedance behavior of electrochemical systems. At present, there are two main models to expound the mechanism of intercalation electrode reaction, namely the adsorption model and the surface layer model.

The adsorption model, also called adatom model or adion model, was usually used to depict the galvanic deposit process of metal ions. It was first used to depict the lithium ions insertion/desertion process of LiTiS_2 by Bruce[19, 20] in the lithium-ion battery field, and then was developed by Kobayashi as well as many others[40, 71, 76, 114]. In this model, the intercalation reaction proceeds in several steps, as shown in **Figure 2-1**: a solvated cation in solution adjacent to the electrode loses part of its solvation sheath and becomes adsorbed, thus forming an adion, on the electrode surface, accompanying by the injection of an electron into the conduction band of the solid host. Subsequently, the partially solvated cation diffuses across the surface of the electrode until it reaches a site at which insertion of the ion can occur, and the ion loses therefore the remaining solvent molecules and enters the host lattice. According to the adsorption model, the EIS spectra of intercalation electrode should involve three parts along with decreasing frequency: (i) a high-frequency dispersion because of the solvated cation losing part of its solvation sheath; (ii) an intermediate frequency semicircle due to the ion losing the remaining solvent molecules and entering the host lattice; (iii) a low-frequency spike of the ionic diffusion. Although the adsorption model can expose some results, it is not widely accepted because of the involvement of solid electrolyte interphase (abbreviated as SEI) with some consequence during the delithiation/lithiation process[106].

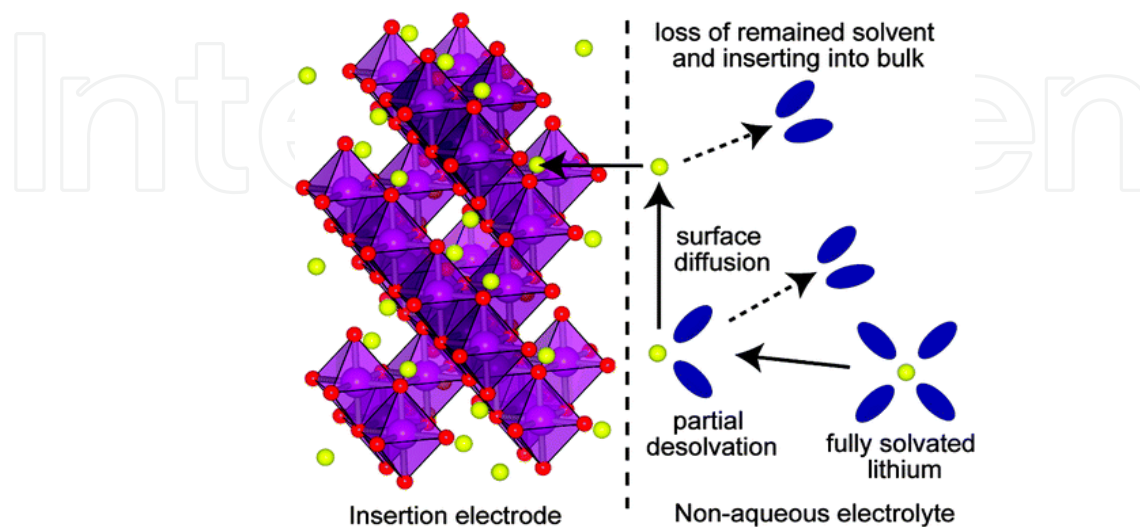


Fig. 2-1. Schematic representation of the adion mechanism of intercalation[76].

The surface layer model (also called SEI model) with approbation was first used to depict the lithium-ion insertion/desertion process of LiCoO_2 by Thomas[102], and developed mainly by Aurbach and co-workers[3-6, 31, 47, 50, 124]. The surface layer model was based on the assumption that electronic conductivity of the intercalation electrode was high and that the power was compacted sufficiently to ensure that each particle was in contact with the aggregate across a solid-solid interface making an ohmic contact of low resistance to electron flow. Under these conditions, the intercalation electrode formed a rough, but continuously interconnected, porous solid of low bulk resistance $R_b \ll R_{el}$ (the bulk electrolyte resistance). According to the surface layer model based on the above assumption, lithium insertion results in a series of complex phenomena. This model reflects the steps involved during lithium-ion insertion: (i) lithium-ion transport in an electrolyte; (ii) lithium-ion migration through the SEI film; (iii) charge-transfer through the electrode/electrolyte interface; (iv) lithium-ion diffusion in an electrode; (v) accumulation-consumption of Li in the electrode, which accompanies phase transition between intercalation stages; (vi) electron transport in an electrode and at an electrode/current collector interface. Among these steps of lithium-ion insertion, the electron transport (vi) and the lithium-ion transport in the electrolyte solution (i) usually do not present semicircle in the frequency range $10^5 \sim 10^2$ Hz range due to their high characteristic frequencies, and these components of resistance appear as a Z' intercept in the Nyquist plot. The process (iv) gives the Warburg impedance, which is observed as a straight line with an angle of 45° from the Z' axis. The process (v) accumulation-consumption of Li in the electrode yields the bulk intercalation capacitance, which is observed as a vertical line, and the other two processes (ii) and (iii) generate their own semicircles at each characteristic frequency, respectively. In the past decades, the modified Voigt-FMG EEC for surface layer model, as shown in **Figure 2-2** and suggested by Aurbach et al.[47], is considered to provide the best account of the lithium-ion insertion process in intercalation electrode.

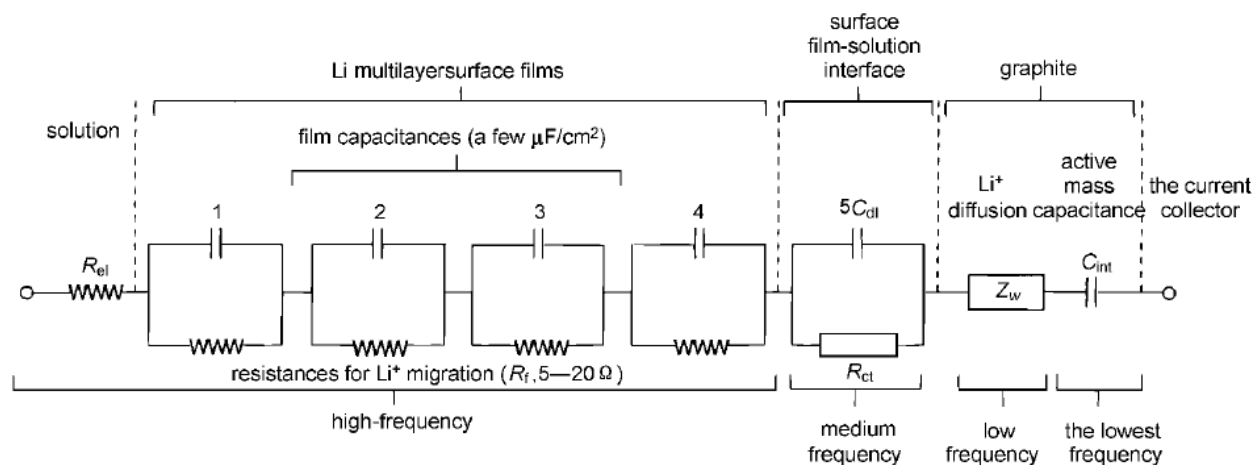


Fig. 2-2. EEC evolved by Aurbach used for analysis of impedance spectra of the lithium-ion insertion/desertion in the intercalation electrode[47].

Yet the above model is a simplification of real situation that the electrode is assumed to be built up of spherical particles of uniform size, and no change of the particle structure or new phase formation in the lithium insertion process. Afterwards, Barsoukov et al.[11, 12] proposed a new model based on single particles for commercial composite electrode, as shown in **Figure 2-3**. They supposed that the electrochemical kinetics characteristic of battery materials was represented by several common steps, as shown in **Figure 2-4**: (i) ionic charge

conduction through electrolyte in the pores of the active layer and electronic charge conduction through the conductive part of the active layer; (ii) lithium-ion diffusion through the surface insulating layer of the active material; (iii) electrochemical reaction on the interface of active material particles including electron transfer; (iv) lithium-ion diffusion in the solid phase and (v) phase-transfer in cases where several phases are present and a capacitive behavior that is related to the occupation of lithium ions, which give a semicircle and straight line perpendicular to Z' axis in the Nyquist plot (commonly below 10^{-2} Hz), respectively.

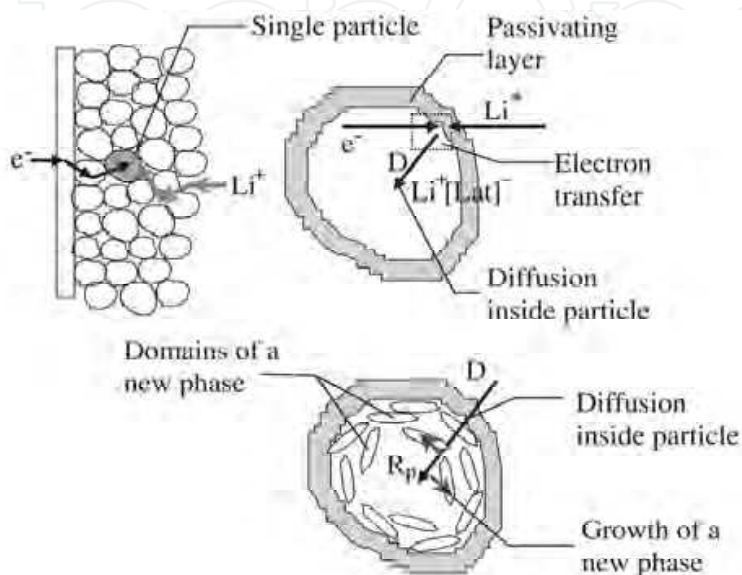


Fig. 2-3. Pictorial representation model for lithium-ion insertion/deinsertion into the intercalation electrode proposed by Barsoukov et al.[12].

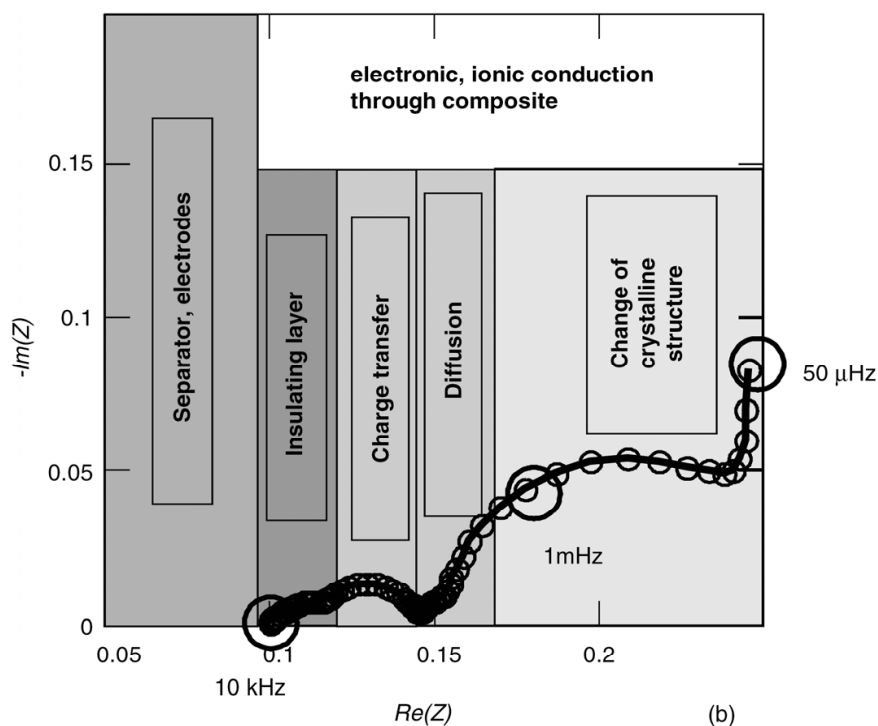


Fig. 2-4. Typical impedance spectra of intercalation electrode proposed by Barsoukov et al.[13].

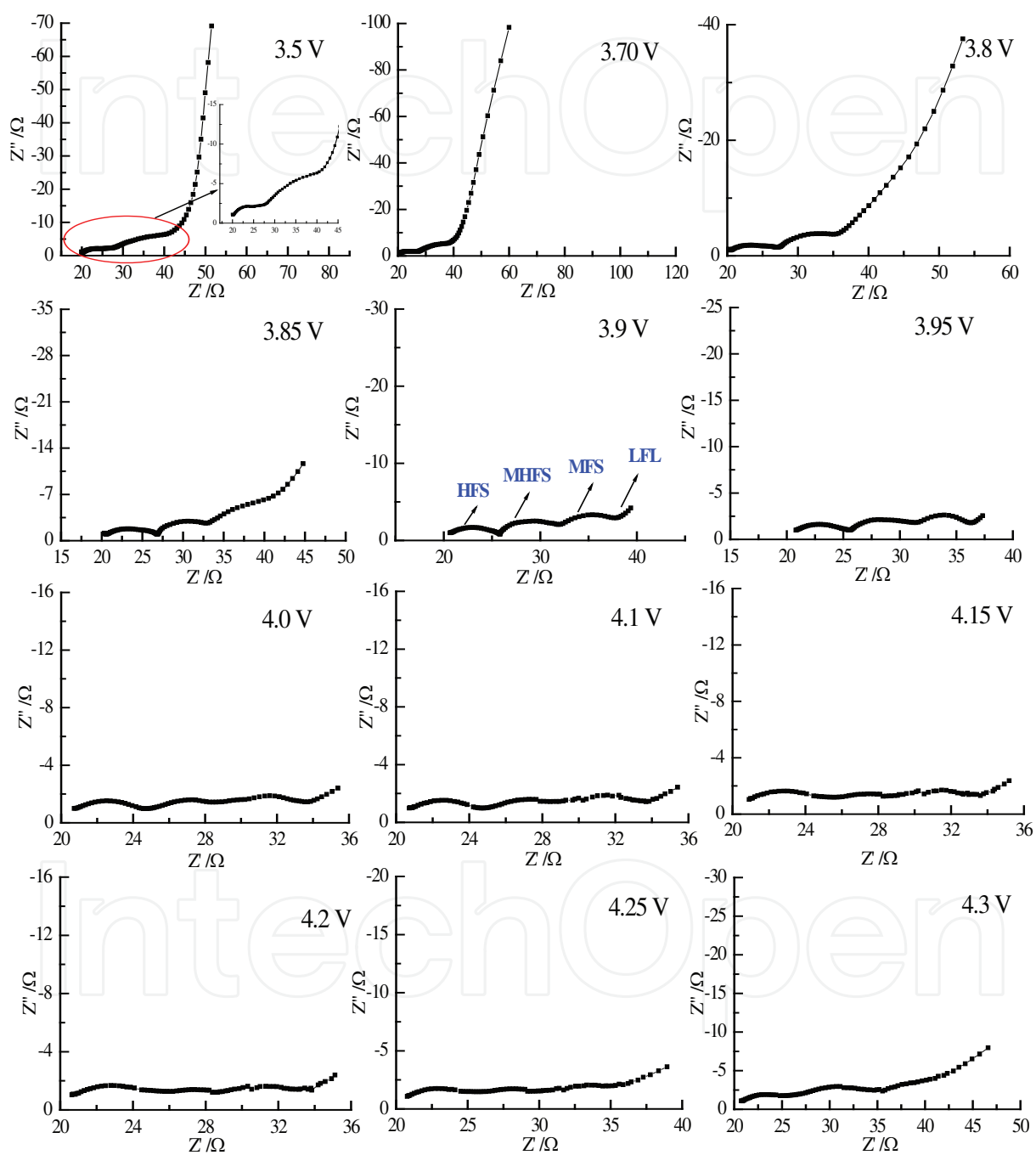


Fig. 2-5. Nyquist plots of the spinel LiMn_2O_4 electrode at various potentials from 3.5 to 4.3 V during the first delithiation[126].

However, many electrochemically active materials, such as LiFePO_4 , LiMn_2O_4 and LiCoO_2 , are not good electronic conductors. As a consequence, it is necessary to add an electronically conductive material such as carbon black. To physically hold the electrode together, a binder is also added. In these cases the electrochemical reaction can only occur at the points where the active material, the conductive diluent and electrolyte meet[110]. So the electrical conductivity of the component materials is one of the most important issues in connection with the intercalation electrode reaction. Nobili and co-workers[25, 61, 72-75] suggested that the Nyquist plots of LiCoO_2 in the delithiated state should involve a third semicircle relating to the electronic properties of the material, however, the three suggested semicircles could not be observed in their experimental results. In our previous work[126], as illustrated in **Figure 2-5**, at intermediate degrees of the first delithiation process in spinel LiMn_2O_4 electrode, three semicircles are observed in the Nyquist diagram, and it was demonstrated that the semicircle in the middle to high frequency range (MHFS) should be attributed to the electronic properties of the material. Therefore, a modified model is put forward, as shown in **Figure 2-6**, and the EEC is illustrated in **Figure 2-7**. In this EEC, R_s represents the ohmic resistance, R_{SEI} and R_{ct} are resistances of the SEI film and the charge transfer reaction. The capacitance of the SEI film and the capacitance of the double layer are represented by the constant phase elements (CPE) Q_{SEI} and Q_{dl} , respectively. The very low frequency region, however, cannot be modeled properly by a finite Warburg element; therefore, it is chosen to replace the finite diffusion by a CPE, i.e., Q_D . The electronic resistance of the material and the associated capacitance used to characterize the electronic properties of the material are represented by R_e and the constant phase elements Q_e . The EIS spectra in the frequency range $10^5 \sim 10^{-2}$ Hz are interpreted in terms of the following physical phenomena in an order of decreasing frequency: (i) a high frequency semicircle (HFS) because of the presence of a surface layer; (ii) a middle to high frequency semicircle (MHFS) related to the electronic

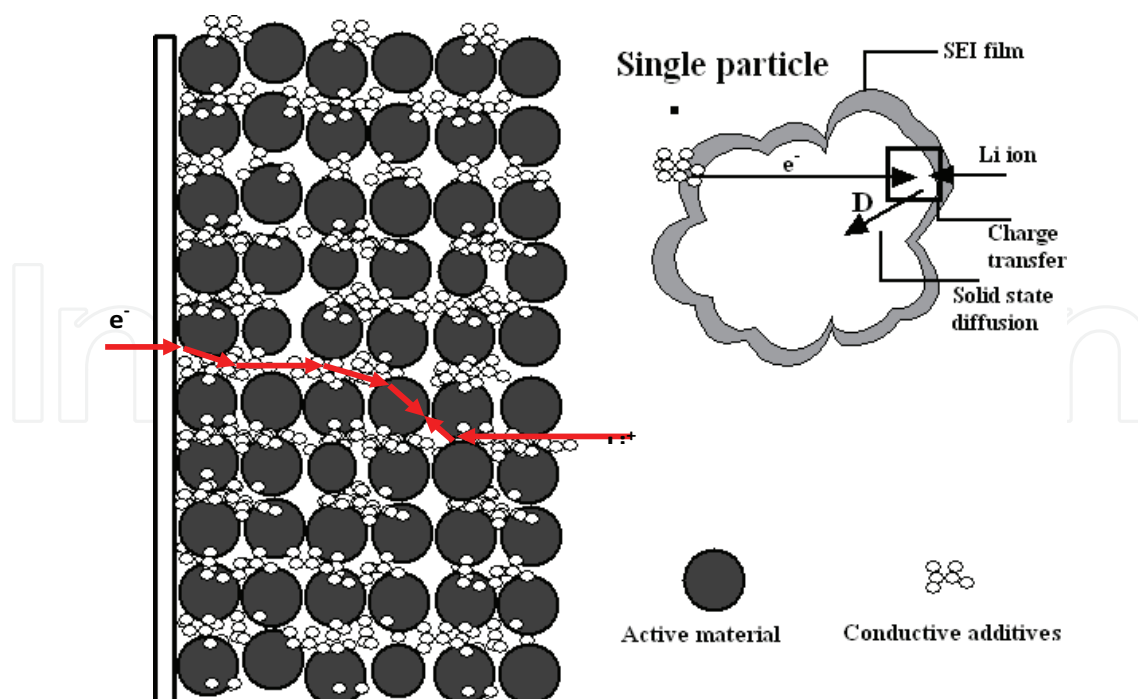


Fig. 2-6. Pictorial representation model for lithium ion insertion/ de-insertion into the intercalation electrode[126].

properties of the material; (iii) a middle frequency semicircle (MFS) associated with charge transfer, and finally, and (iv) the very low frequency incline line attributed to the solid state diffusion.

Although the adsorption model or surface layer model both can fit partially some results, a debate is still open on that whether or not the solvated/lost solvated or the migration of lithium ions through the SEI film is the rate determining step in the transport of lithium-ion? Namely, what should be the origin of the semicircle in the high frequency range (HFS)? On the base of the adsorption model, the HFS is attributed to the solvated/lost solvated of lithium ions; while according to the surface layer model, the HFS is ascribed to the migration of lithium ions through the SEI film. So, it needs to be further investigated.

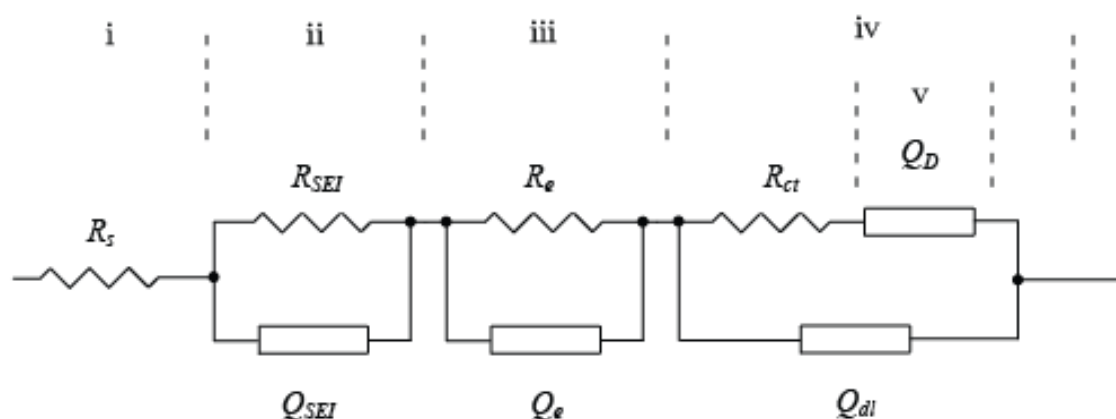


Fig. 2-7. Equivalent circuit proposed for analysis of the intercalation electrode during the charge-discharge processes[126].

3. Kinetic models for the lithiation and delithiation of simple binary transition metal compounds

In 2000, Poizot et al.[84] reported for the first time that lithium could be stored reversibly in some simple binary transition metal (TM) oxides MO_x ($M=Fe, Co, Ni, \text{ etc.}$) through a heterogeneous conversion reaction, i.e. $MO_x + 2xLi \rightarrow M^0 + xLi_2O$, which is different from the intercalation/deintercalation mechanism. Later, reversible lithium storage was also observed in transition metal fluorides as well as sulfides, nitrides, selenides and phosphides[7, 8, 26, 63, 81, 82, 89, 94, 116]. As opposed to intercalation reactions, the reversible conversion process enables the full redox utilization of the transition metal and has 2-4 times the specific capacity of intercalation compounds as high as $600-1000 \text{ mAh.g}^{-1}$ [54]. Therefore, as potential alternatives for intercalation compounds, transition metal oxides as well as other transition metal compounds attract lots of attention in recent years.

As a new type of reaction, the kinetic behavior of the conversion reaction is not very clear and remains to be revealed. **Figure 3-1** and **3-2** show Nyquist plots of the NiF_2/C composites electrode prepared through high energy mechanical milling during the first discharge and charge process, respectively. It can be seen that the typical EIS characteristics appeared with three semicircles in the Nyquist diagram at 1.6 V, similar to that of intercalation electrode. However, most metal fluorides such as NiF_2 are insulators with large band gap, the fitted values of the semicircle in the middle frequency region (MFS), with the

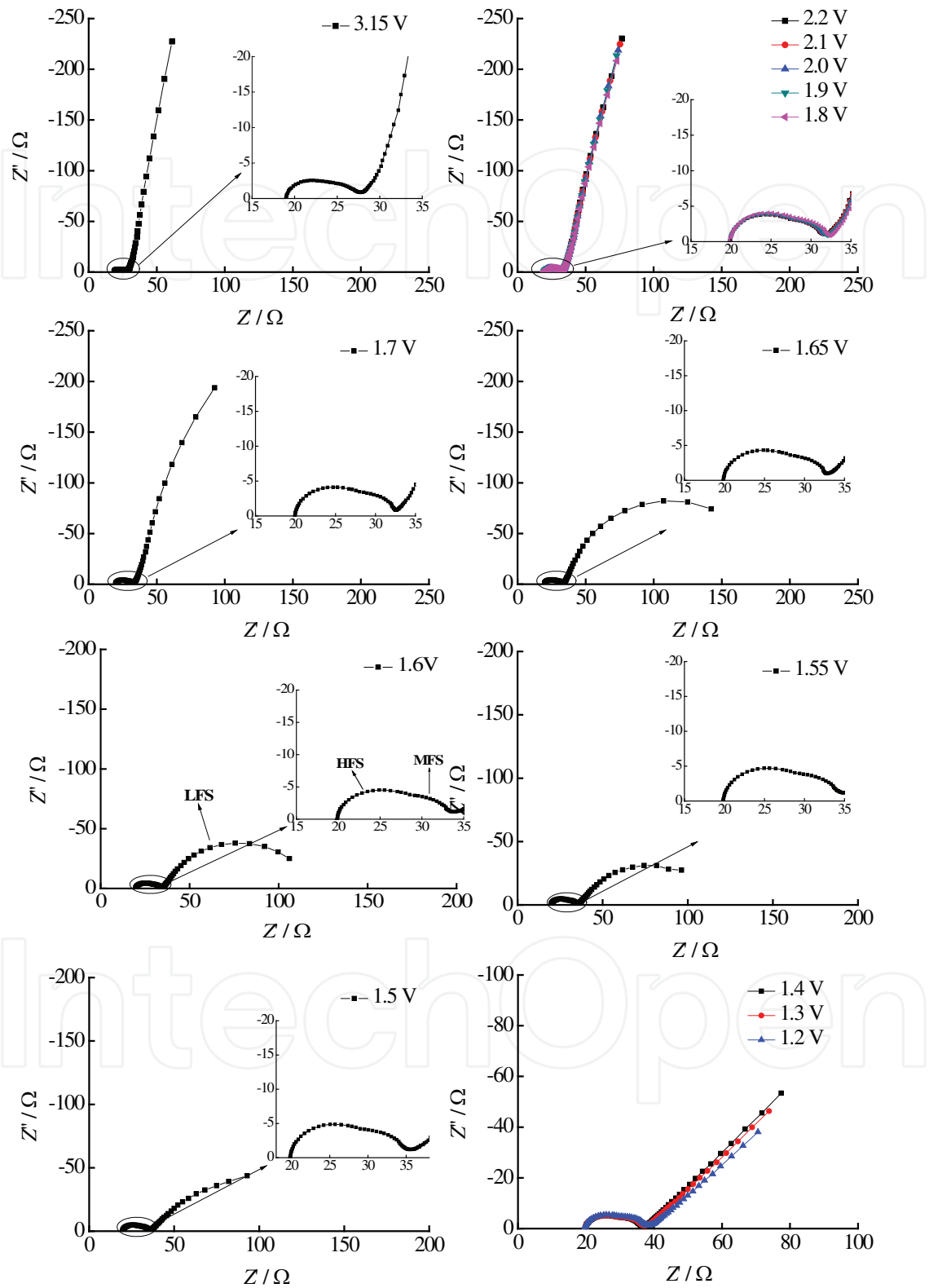


Fig. 3-1. Nyquist plots of the NiF₂/C composites electrode during the first discharge process[88].

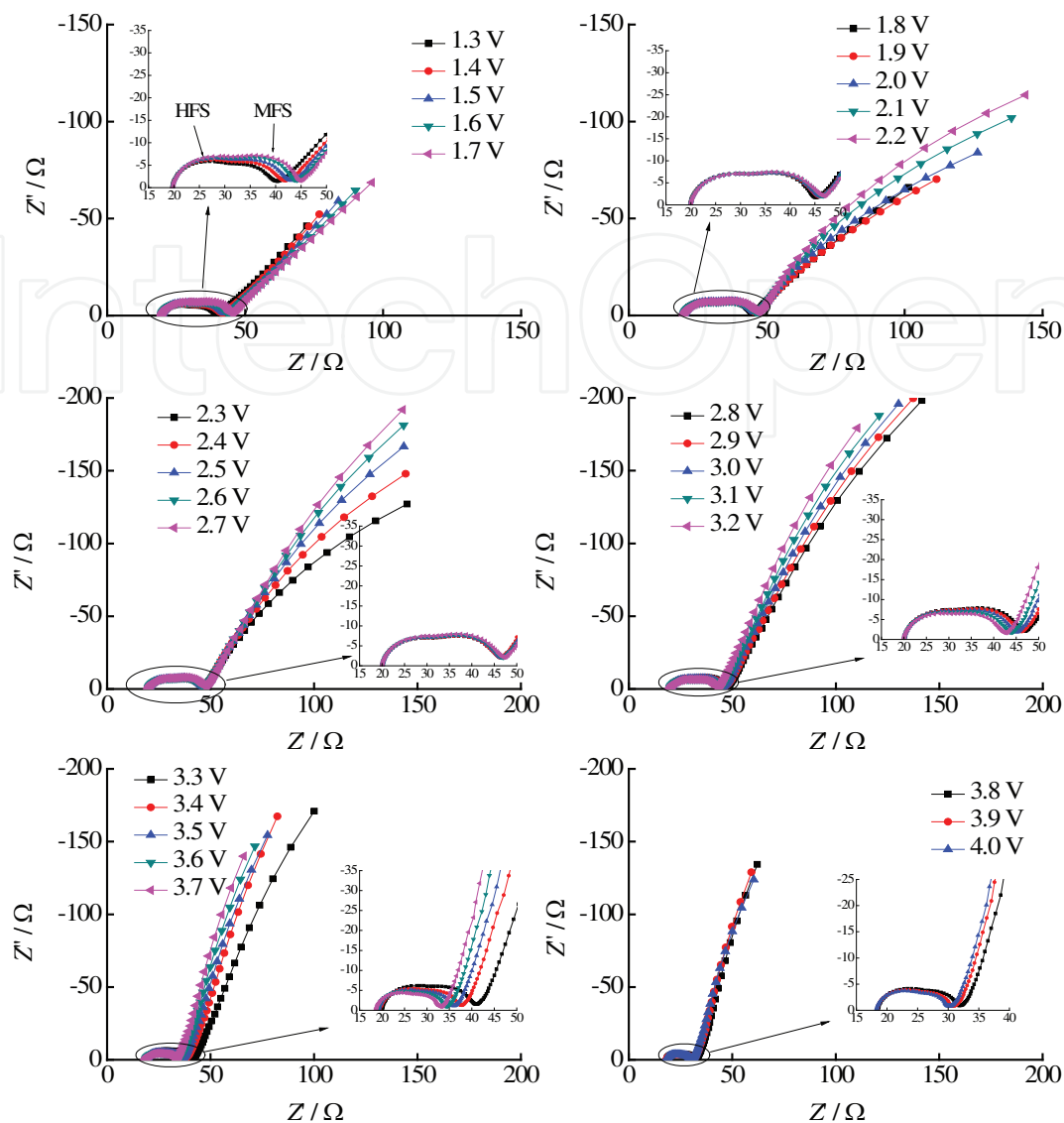


Fig. 3-2. Nyquist plots of the NiF_2/C composites electrode during the first charge process[88].

value of only scores of ohms, could not be the reflection of the electronic resistance of NiF_2 , and it has been demonstrated that the MFS should be related to the contact between conductive agents and active materials. Based on the above experimental results, a new model (**Figure 3-3**) is put forward in our recent studies[88]. The EIS is interpreted in terms of the following physical phenomena in an order of decreasing frequency: firstly ionic charges conduct through electrolyte and lithium ions diffuse through the SEI film to the surface of the NiF_2 ; To maintain electrical neutrality of particles, electrons conduction along the external circuit, conductive agents, and the contact points between NiF_2 and C, then hop on the surface of NiF_2 . Later the charge transfer process takes place close to the carbon particles. But for the diffusion process, because F^- could migrate in the NiF_2 particles[2] and compete favorably with Li^+ [120], there may exist two ways: (i) Li^+ diffuses to contact points to form LiF along the particle surface; (ii) F^- migrates further from the carbon, through the NiF_2 phase, or along the newly formed Ni-NiF_2 interfaces, so as to the surface of NiF_2 and form LiF with Li^+ .

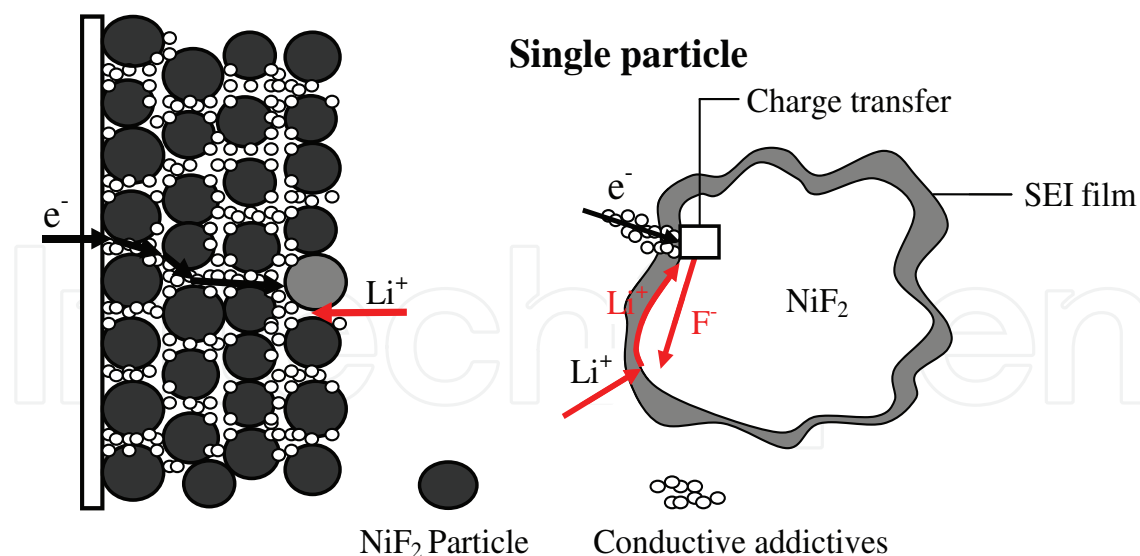


Fig. 3-3. Pictorial representation model for lithium-ion insertion/ de-insertion into NiF_2/C composite electrode based on conversion reaction[88].

4. The potential and temperature dependence of the kinetic parameters

The main problem remaining in the practical application of EIS is its ambiguity: many physically different procedures or separate stages of a complicated process show similar features in terms of impedance spectroscopy. A classical electrochemical system contains processes such as electron-transfer, diffusion and absorption of reacting species, and elucidating these processes could be easy if all absorption sites have the same energy, i.e. the electrode surface is energetically homogeneous. However, the processes occurring in practical ion insertion electrodes are much more complicated compared to the classical systems. The practical ion insertion electrodes are composite materials, in which the active mass particles are bound to a current collector with a polymeric binder such as polyvinylidene fluoride (PVDF). In addition, the composite electrodes have to contain a conductive additive, usually carbon black. The electrodes are regularly prepared from slurry of the particles and the binder in an organic solvent, which is spread on the current collector, followed by drying. The final shape of the electrode is obtained by applying some pressure to the electrode. So the shape and value of the resistance in the impedance spectrum should be affected by the amount of conductive additive in the composite materials, the contact between the electrode film and the current collector, the solvent, particle size, thickness of electrode, and stack pressure[23, 48, 93]. Without systematic and integrated comparison of EIS spectra of these processes, incorrect interpretation may arise. So it is important to determine the physical processes corresponding to time constants ranging via theoretical analysis and contrast tests in detail.

4.1 Kinetic parameters for lithium-ion migration through the SEI film

The SEI film is a key element of traditional Li-ion batteries and plays an important role in the electrochemical performance of the electrode material and a battery[113]. The SEI film prevents lithium from being intercalated in the solvated state, which leads to the exfoliation (swelling) of the carbon. In addition, the SEI film inhibits also the further reduction of electrolyte by active lithium and thus limits the degradation of the electrolyte. The

semicircle in the Nyquist plots in the high frequency range is commonly attributed to lithium-ion migration through the SEI film, and its characteristic parameters are the resistance due to Li ions migration, R_{SEI} , and geometric capacitance of the surface films, C_{SEI} .

The resistance and capacitance values corresponding to the migration of Li ions through the SEI film can be described by Eq. (4-1) and (4-2)

$$R_{SEI} = \rho l / S \quad (4-1)$$

$$C_{SEI} = \varepsilon S / l \quad (4-2)$$

where l is the thickness of the SEI film, S the electrode surface area, ρ the resistivity, and ε the permittivity of the SEI film. If we assume that the surface S , permittivity ε , and resistivity ρ remain constant, it is clear that a thickness increase will lead to a resistance increase, and to a decrease in capacitance.

4.1.1 The growth rate of SEI film

A simple model for SEI film growth can be formulated similarly to the growth of oxides on metals. A metal exposed to air reacts to form an oxide which helps passivate the surface and slows further reaction. Similarly, lithiated graphite exposed to electrolyte reacts to form an SEI film which helps passivate the surface and slows further reactions. Lawless reviewed numerous models of oxide growth on metals which he showed followed a huge variety of rate laws[44]. The simplest of these is the “parabolic growth law” which assumes that the rate of increase in the thickness of the passivating layer, l , is inversely proportional to the thickness of the layer

$$dl/dt = k/l \quad (4-3)$$

where k is a proportionally constant. This can be rewritten as

$$l dl = k dt \quad (4-4)$$

and the integration yields

$$1/2 l^2 = kt + C \quad (4-5)$$

If the thickness is taken $x=0$ at $t=0$, then the constant, C is zero and one can write

$$l = (2kt)^{1/2} \quad (4-6)$$

The rate of change of the thickness of the passivating layer is formulated by combining Eqs. (4-3) and (4-6), i.e.

$$dl/dt = (1/2k)^{1/2} t^{-1/2} \quad (4-7)$$

In a Li/graphite cell, it is believed that the SEI film begins to form as lithium is transferred electrochemically to the graphite electrode. With continuously cycling more and more Li is irreversibly consumed as the SEI film becomes more and more thick. The total amount of Li consumed is directly proportional to the SEI film thickness, which might be described by Eq.

(4-6). The amount of lithium consumed by SEI film growth is directly proportional to the irreversible capacity in each cycle, which might be described by Eq. (4-7). Many researchers studying the failure of Li-ion batteries have identified this capacity loss vs $t^{1/2}$ (or equivalent) relationship and have demonstrated that their models fit experimental data very well [16, 85, 92, 95, 122].

4.1.2 The potential dependence of the SEI film resistance

According to the SEI model mentioned, it is possible to use Eq. (4-8) describing the migration of ions in a solid crystal under external field [80]. It is assumed that the thickness (l) is larger than the space charge lengths in the SEI, and there is no change in the concentration or molality of the mobile lattice defects through the SEI film.

$$i = 4zFacv \exp(-W / RT) \sinh(azFE / RT) \quad (4-8)$$

in Eq. (4-8) a = half-jump distance, v = vibration frequency of the ion in the crystal, c = concentration of the lattice cationic defect, z = the valance of the mobile ion, W = a barrier energy for jumping, E = electricfield, F = Faraday constant. The assumption that the migration of the cation in the SEI is the rate determining step (rds) means the largest fraction of the electrode overpotential (η) will develop on the SEI, i.e.

$$\eta = \eta_{SEI} = El \quad (4-9)$$

For low field conditions, Eq. (4-8) can be linearization into Eq. (4-10)

$$i = (4z^2F^2a^2cv / RTl) \exp(-W / RT) \eta \quad (4-10)$$

thus

$$R_{SEI} = (RTl / 4z^2F^2a^2cv) \exp(W / RT) \quad (4-11)$$

or

$$\ln R_{SEI} = \ln(RTl / 4z^2F^2a^2cv) + W / RT \quad (4-12)$$

The relation between $\ln R_{SEI}$ and $1/T$ is linear given by Eq. (4-12), and W can be obtained from the line gradient.

According to Eq. (4-12), the energy barriers for the ion jump relating to migration of lithium ions through the SEI film of the spinel LiMn_2O_4 electrode in 1 mol/L LiPF_6 -EC (ethylene carbonate): DEC (diethyl carbonate) was determined to be 15.49 kJ/mol [109], and that of LiCoO_2 electrode in 1 mol/L LiPF_6 -EC:DEC:DMC (dimethyl carbonate) and 1 mol/L LiPF_6 -PC (propylene carbonate):DMC+5% VC (vinylene carbonate) electrolyte solutions were calculated to be 37.74 and 26.55 kJ/mol [125], respectively, in our previous studies.

4.2 Kinetic parameters for electron charge conduction

4.2.1 The electronic properties of intercalation materials

Among the characteristics of insertion materials, the electrical conductivity of the component materials is one of the most important issues in connection with the rate

performance of batteries. In addition to such practical importance, conductivity measurements during the lithium insertion (and extraction) reaction would be an attractive approach for the study of the variation in the electronic structure of the materials as a function of lithium content[68, 69]. The semicircle in the Nyquist plots in the middle to high frequency range is commonly ascribed to the electronic properties of intercalation materials, and its characteristic parameters are the electronic resistance of the insertion materials R_e and geometric capacitance of the insertion materials C_e .

According to the Ohm's law, the electrical conductivity can be obtained through the equality (4-13):

$$R_e = l / (\sigma S) \quad (4-13)$$

where σ is the conductivity, l is the thickness of the electrode film, and S is the area of the electrode film.

4.2.1.1 The temperature dependence of R_e

All cathode materials for lithium-ion batteries have semiconductor features. Electrical conduction in a semiconductor is a thermally activated phenomenon and usually follows an Arrhenius type relationship as shown below[99]:

$$\sigma T = \sigma_0 \exp(-E_a/k_B T) \quad (4-14)$$

where σ is the electrical conductivity, σ_0 is the pre-exponential factor, E_a is the activation energy, k_B is the Boltzmann constant and T is the temperature.

On the substitution of Eq. (4-14) in Eq. (4-13), one gets

$$R_e = \frac{lT}{S\sigma_0} \exp(E_a / k_B T) \quad (4-15)$$

$\ln 1/T$ is acted by Taylor series expansion and ignored the high-order component, Eq. (4-15) can become into

$$\ln R_e = \ln \frac{l}{S\sigma_0} + \frac{(E_a - k_B)}{k_B T} + 1 \quad (4-16)$$

Eq. (4-16) presents explicitly that when $1/T \rightarrow 0$ and constant electrode potential, the relation between $\ln R_e$ and $1/T$ is linear, and E_a can be obtain from the line gradient.

4.2.1.2 The potential dependence of R_e

As noted above, all cathode materials for lithium-ion batteries have semiconductor features, and can be to be divided into n -type semiconductor and p -type semiconductor, which have different potential dependence of R_e .

It is well known [93, 108, 123] that LiCoO_2 is a p -type semiconductor (band-gap $E_g = 2.7$ eV)[105], while Li_xCoO_2 exhibits a metal-like behavior for $x < 0.75$. Li_xCoO_2 is predicted to have partially filled valence bands for x lower than 1.0[104]. For each Li removed from LiCoO_2 lattice, an electron hole is created within the valence band. Namely,

$$p = 1 - x \quad (4-17)$$

where p is the concentration of electron hole. We may expect that there will be sufficient holes, when x is below 0.75, to allow for a significant degree of screening. And in this regime, the hole states in the valence bands are likely to be delocalised so that Li_xCoO_2 exhibits metallic-like electronic properties, namely, the existence of a drastic change of the electronic conductivity occurs at early stage of lithium deintercalation, which may be caused by a transition from insulator to metal (or so called metal-insulator transition). This behavior is clearly observed in infrared absorption spectra where a strong absorption by holes occurs at low wavenumbers[38]. Accordingly, the variation with potential of electronic conductivity of LiCoO_2 in the charge-discharge process may be divided into three regions: (1) the region in which Li_xCoO_2 has a semiconductor-like behavior; (2) the region in which the hole states in the valence bands are likely to be delocalised; (3) the region in which Li_xCoO_2 has a metal-like behavior.

The general expression for the electronic conductivity for p-type semiconductor is given by Eq. (4-18).

$$\sigma = pq\mu \quad (4-18)$$

where μ is carrier hole mobility, and q is electron charge.

The Langmuir insertion isotherm could be used for lithium-ion deintercalation from LiCoO_2 hosts by assuming that the interaction between the intercalated species and the host material as well as the interaction between the intercalated are absent. Thus, the intercalation level, x , is given by[45]:

$$x/(1-x) = \exp[f(E-E_0)] \quad (4-19)$$

where $f=F/RT$ (F and R , Faraday and gas constant respectively, T , absolute temperature), E and E_0 define the electrode's real and standard potentials in the equilibrium.

On the substitution of Eq. (4-17) in Eq. (4-19), one gets

$$p = 1 / \{1 + \exp[f(E-E_0)]\} \quad (4-20)$$

While on the substitution of Eq. (4-13) and Eq. (4-18) in Eq. (4-20), one has

$$\ln R_e = \ln(S / q\mu l) + \ln\{1 + \exp[f(E-E_0)]\} \quad (4-21)$$

$\ln\{1 + \exp[f(E-E_0)]\}$ is acted by Taylor series expansion. If the high-order component is ignored, we have

$$\ln R_e = \ln(2S / q\mu l) + \frac{1}{2} f(E-E_0) \quad (4-22)$$

It can be seen from Eq. (4-22) that, the value of $\ln R$ shows a linear dependence on electrode potential. Therefore the variation of the electronic conductivity of LiCoO_2 in the charge-discharge process with potential may be divided into three different parts: (i) when Li_xCoO_2 has a semiconductor-like behavior, the value of $\ln R_e$ shows a linear dependence on electrode potential; (ii) when the hole states in the valence bands are likely to be delocalised, the value of $\ln R_e$ increases or decreases drastically with electrode potential; (iii) when Li_xCoO_2 has a metal-like behavior, the value of $\ln R_e$ also exhibits a linear dependence on electrode potential.

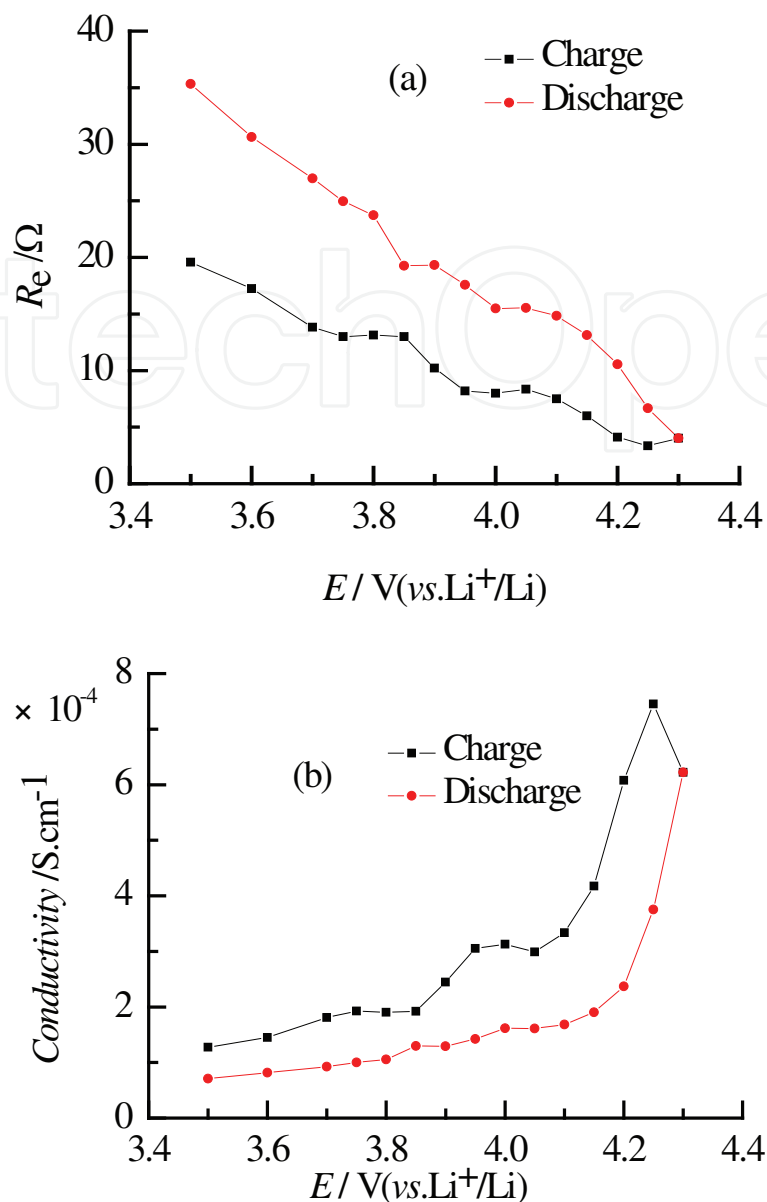


Fig. 4-1. Variations of R_e (a) obtained from fitting the experimental impedance spectra of the spinel LiMn_2O_4 electrode and the conductivity (b) derived from R_e with electrode potential during the first charge-discharge cycle[126].

While spinel LiMn_2O_4 is an n -type semiconductor, which is a mixed-valence ($\text{Mn}^{3+}/\text{Mn}^{4+}$) compound and its electronic conduction takes place by electron-hopping between high-valence (Mn^{4+}) and low-valence (Mn^{3+}) cations[62, 83]. Conductivity of this type would be governed by the concentration of carriers (electrons from Mn^{3+}) and the hopping length (Mn-Mn interatomic distance). The number of electron carriers decreases proportionally with the degree of de-lithiation coupled with oxidation of Mn^{3+} to Mn^{4+} . On the other hand, the Mn-Mn distance in the spinel structure is reduced by delithiation. Variations of R_e obtained from fitting the experimental impedance spectra of the spinel LiMn_2O_4 electrode and the conductivity derived from R_e with electrode potential during the first charge-discharge cycle are shown in **Figure 4-1**. The conductivity derived from R_e is in the range of 10^{-4} $\text{S}\cdot\text{cm}^{-1}$, being roughly in agreement with previous reports[39, 70]. The electronic

resistance of the material in the charge and discharge process has the same change relationship with potential, namely, R_c decreases with the increase of the electrode polarization potential in the charge process, and increases with the decrease of the electrode polarization potential, indicating that the effect of the contraction of hopping length predominated over the decrease of the numbers of electron carriers.

4.2.2 The potential dependence of Schottky contact resistance

The semicircle in the Nyquist plots of binary transition metal (TM) compounds in the middle frequency range is commonly ascribed to the Schottky contact and its characteristic parameters are the resistance R_c and capacitance of the Schottky contact. According to thermionic emission diffusion theory, a Schottky contact behaviour can be described by the equation which takes into account the defects of lattice, electric field, tunneling effects, the presence of an interfacial layer, and carrier recombination in the space charge region of the metal-semiconductor contact as given by [21, 86, 98]:

$$I = I_0 \exp\left(\frac{qE}{nk_B T}\right) \left[1 - \exp\left(\frac{-qE}{k_B T}\right)\right] \quad (4-23)$$

where I_0 is the saturation current, q the electronic charge, k Boltzmann constant, T the absolute temperature, E the applied bias voltage, n is the ideal factor. The expression for the saturation current, I_0 is:

$$I_0 = AA^* T^2 \exp\left(-\frac{q\Phi_B}{k_B T}\right) \quad (4-24)$$

where A is the Schottky contact area, A^* the effective Richardson constant, and $q\Phi_B$ is the Schottky barrier height. When $E > 3kT / q$, Eq. (4-24) can be simplified as,

$$I = I_0 \exp\left(\frac{qE}{nk_B T}\right) \quad (4-25)$$

According to the Ohm's Laws, the Schottky contact resistance R_c can be presented in the following form:

$$R_c = \left(\frac{dI}{dE}\right)^{-1} \quad (4-26)$$

substitute Eq. (4-25) into Eq. (4-26), R can be expressed as following.

$$R_c = \left(I_0 \frac{q}{nk_B T}\right)^{-1} \exp\left(-\frac{qE}{nk_B T}\right) \quad (4-27)$$

When the contact media do not change, A^* and Φ_B could be considered to be the same, Eq. (4-27) could be written as:

$$R_c = C \exp\left(-\frac{qE}{nk_B T}\right) \quad (4-28)$$

where C is constant. Therefore change Eq. (4-28) to linear equation by logarithm, we can obtain finally the following expression:

$$\ln R_c = \ln C - \frac{qE}{nk_B T} \quad (4-29)$$

The plot of $\ln R_c$ versus E should give a straight line with the slope = $-q/nk_B T$ and y-intercept at $\ln C$ on condition that no change occur with contact media.

4.3 Kinetic parameters for the charge transfer process

Among several processes of lithium ion and electron transport, the charge transfer at an electrode/electrolyte interface is an essential process of the charge-discharge reaction of lithium ion batteries. The semicircle in the Nyquist plots in the low frequency range is commonly attributed to the charge transfer process, and its characteristic parameters are the charge-transfer resistance, R_{ct} , and the double layer capacitance, C_{dl} .

4.3.1 The potential dependence of R_{ct}

The electrochemical reaction of intercalation electrode is given by Eq. (4-30)



where M is the transition metal.

Suppose that the velocity of the forward reaction r_f (lithiation in intercalation electrode) is proportional to $c_{\max}(1-x)$ and the concentration (M_{Li^+}) of lithium-ion in the electrolyte near the electrode. $c_{\max}(1-x)$ is the insertion sites on the intercalation electrode surface not occupied by lithium ions, x is the insertion level, c_{\max} (mol/cm³) is the maximum concentration of lithium ion in intercalation electrode. Then, the velocity of the backward reaction rate r_b is proportional to $c_{\max}x$, $c_{\max}x$ is the sites already occupied by lithium ions. r_f and r_b can be written as [10, 128]

$$r_f = k_f c_{\max} (1-x) M_{Li^+} \quad (4-31)$$

$$r_b = k_b c_{\max} x \quad (4-32)$$

Therefore:

$$i = r_f - r_b = n_e F c_{\max} [k_f (1-x) M_{Li^+} - k_b x] \quad (4-33)$$

where n_e is the number of electron exchange in the processes of lithium ion insertion and extraction, F is the Faraday constant; k_f and k_b are the velocity constants of the forward and backward reactions.

The molar intercalation energy ΔG_{int} of the intercalation electrode can be expressed as

$$\Delta G_{\text{int}} = a + mx \quad (4-34)$$

where a is the constant about the interaction energy between an intercalated ion and a host lattice near it, and m is the constant about the interaction energy between two intercalated ions in different sites.

According to the activated complex theory, k_f and k_b can be expressed from [53]

$$k_f = k_f^0 \exp\left[\frac{-\alpha(n_e FE + \Delta G_{\text{int}})}{RT}\right] \quad (4-35)$$

$$k_b = k_b^0 \exp\left[\frac{(1-\alpha)(n_e FE + \Delta G_{\text{int}})}{RT}\right] \quad (4-36)$$

with a representing symmetry factor for the electrochemical reaction, and k_f^0 and k_b^0 can be written in the Arrhenius form

$$k_f^0 = A_f \exp\left(\frac{-\Delta G_{0f}}{RT}\right) \quad (4-37)$$

$$k_b^0 = A_b \exp\left(\frac{-\Delta G_{0b}}{RT}\right) \quad (4-38)$$

Substitute Eqs. (4-35) and (4-36) into Eq. (4-33), the current i can be obtained in the following expression

$$i = n_e F c_{\text{max}} k_f^0 (1-x) M_{\text{Li}^+} \exp\left[\frac{-\alpha(n_e FE + \Delta G_{\text{int}})}{RT}\right] - n_e F c_{\text{max}} k_b^0 x \exp\left[\frac{(1-\alpha)(n_e FE + \Delta G_{\text{int}})}{RT}\right] \quad (4-39)$$

when the forward reaction r_f equal the backward reaction r_b , that is to say $i=0$, so the exchange current density i_0 can be obtained

$$i_0 = n_e F c_{\text{max}} k_f^0 (1-x) M_{\text{Li}^+} \exp\left[\frac{-\alpha(n_e FE + \Delta G_{\text{int}})}{RT}\right] = n_e F c_{\text{max}} k_b^0 x \exp\left[\frac{(1-\alpha)(n_e FE + \Delta G_{\text{int}})}{RT}\right] \quad (4-40)$$

Thus

$$i_0 = n_e F c_{\text{max}} k_0 (M_{\text{Li}^+})^{(1-\alpha)} (1-x)^{(1-\alpha)} x^\alpha \quad (4-41)$$

where k_0 is the standard reaction speed constant and k_0 can be expressed as

$$k_0 = k_f^0 \exp\left[\frac{-\alpha(n_e FE_0 + \Delta G_{\text{int}})}{RT}\right] = k_b^0 \exp\left[\frac{(1-\alpha)(n_e FE_0 + \Delta G_{\text{int}})}{RT}\right] \quad (4-42)$$

The charge transfer resistance can be defined as

$$R_{\text{ct}} = RT/n_e F i_0 \quad (4-43)$$

Substitute Eq. (4-41) into Eq. (4-43), we get

$$R_{ct} = \frac{RT}{n_e^2 F^2 c_{\max} k_0 (M_{Li^+})^{(1-\alpha)} (1-x)^{(1-\alpha)} x^\alpha} \quad (4-44)$$

Suppose that the delithiation/lithiation process in intercalation electrode is invertible, namely, $\alpha = 0.5$, the Eq. (4-44) can be expressed as

$$R_{ct} = \frac{RT}{n_e^2 F^2 c_{\max} k_0 (M_{Li^+})^{0.5} (1-x)^{0.5} x^{0.5}} \quad (4-45)$$

Eq. (4-45) predicts clearly a rapid increase in R_{ct} with the decrease of x as $x < 0.5$, a rapid decrease in R_{ct} with the increase of x as $x > 0.5$, and the minimum R_{ct} will be reached at $x = 0.5$.

At the beginning of lithium ion inserts into or the very end of lithium ion extracts from the active mass during the electrochemical processes, that is to say, for very low insertion level ($x \rightarrow 0$). Eq. (4-19) takes the form

$$x = \exp[f(E - E_0)] \quad (4-46)$$

Substitute Eq. (4-46) into Eq. (4-44), we get

$$R_{ct} = \frac{RT}{n_e^2 F^2 c_{\max} k_0 (M_{Li^+})^{(1-\alpha)}} \exp\left[\frac{-\alpha F(E - E_0)}{RT}\right] \quad (4-47)$$

changing Eq. (4-47) to linear equation by logarithm, we can obtain finally the following expression:

$$\ln R_{ct} = \ln \frac{RT}{n_e^2 F^2 c_{\max} k_0 (M_{Li^+})^{(1-\alpha)}} - \frac{\alpha F(E - E_0)}{RT} \quad (4-48)$$

Eq. (4-48) presents explicitly that when $x \rightarrow 0$, $\ln R_{ct} \sim E$ shows a linear variation and the symmetry factors of charge transfer in electrochemical kinetics, α , can be calculated from the straight line slope. By using Eq. (4-48), the symmetry factor of charge transfer of lithium-ion insertion-desertion in LiCoO_2 is determined as 0.5 in our previous studies[128], and that of lithium-ion insertion-desertion in graphite materials is determined as 0.56 by Holzapfel et al.[36].

4.3.2 The temperature dependence of R_{ct}

According to Eq. (4-37), Eq. (4-42) and Eq. (4-44), we can get

$$R_{ct} = \frac{RT}{n_e^2 F^2 c_{\max} A_f (M_{Li^+})^{(1-\alpha)} (1-x)^{(1-\alpha)} x^\alpha} \times \exp\left[\frac{\Delta G_{0c} + \alpha(nFE_0 + \Delta G_{\text{int}})}{RT}\right] \quad (4-49)$$

the intercalation-deintercalation reaction active energies ΔG can be expressed from

$$\Delta G = \Delta G_{0c} + \alpha(nFE_0 + \Delta G_{\text{int}}) = \Delta G_{0c} + \alpha(nFE_0 + a + gx) \quad (4-50)$$

Substitute Eq. (4-50) into Eq. (4-49), we get

$$R_{ct} = \frac{RT}{n_e^2 F^2 c_{\max} A_f (M_{Li^+})^{(1-\alpha)} (1-x)^{(1-\alpha)} x^\alpha} \times \exp\left(\frac{\Delta G}{RT}\right) \quad (4-51)$$

and Eq. (4-51) can become as

$$\ln R_{ct} = \ln \frac{R}{n_e^2 F^2 c_{\max} A_f (M_{Li^+})^{(1-\alpha)} (1-x)^{(1-\alpha)} x^\alpha} + \frac{\Delta G}{RT} - \ln \frac{1}{T} \quad (4-52)$$

$\ln 1/T$ is acted by Taylor series expansion and ignored the high-order component, one gets

$$\ln R_{ct} = \ln \frac{R}{n_e^2 F^2 c_{\max} A_f (M_{Li^+})^{(1-\alpha)} (1-x)^{(1-\alpha)} x^\alpha} + \frac{(\Delta G - R)}{RT} + 1 \quad (4-53)$$

Eq. (4-53) presents explicitly that when $1/T \rightarrow 0$ and at constant electrode potential, the relation between $\ln R_{ct}$ and $1/T$ is linear and ΔG can be obtain from the line gradient.

According to Eq. (4-53), the intercalation-deintercalation reaction active energies of LiCoO_2 are calculated in our previous studies[128] to be 68.97 and 73.73 kJ/mol, respectively, in 1 mol/L LiPF_6 -EC: DEC: DMC and 1 mol/L LiPF_6 -PC: DMC+5%VC electrolyte solutions, and that of $\text{Li}_{4/3}\text{Ti}_{5/3}\text{O}_4$ was determined at 48.6 ± 0.3 kJ·mol⁻¹ in PC-based electrolyte and 44.0 ± 1.2 kJ·mol⁻¹ in EC +DEC-based electrolyte by Doi et al.[29].

4.4 Diffusion coefficients

Normally, the concentration of the lithium ions in solution is nearly 1mol·L⁻¹ and the diffusion coefficient, D , is about 10⁻⁵cm²·s⁻¹, and the values of these two parameters are both bigger than that in intercalation compounds (concentration $\sim 10^{-2}$ mol·L⁻¹, $D \sim 10^{-10}$ cm²·s⁻¹). Therefore, the charge transfer in the liquid phase could be neglected. The feature of EIS of intercalation compounds electrode in the low-frequency region shows an inclined line. It represents the Warburg impedance (Z_w), which is associated with lithium ions diffusion in the intercalation particles. Ho and Huggins et al.[35] first applied EIS to investigate the intercalation reaction of the intercalation electrode, and they did some theoretical derivations in order to get the expression of Z_w . Thus, the diffusion coefficient D can be calculated form Z_w .

For the case of semi-infinite diffusion

$$Z_w = \frac{B}{\sqrt{\omega}} - j \frac{B}{\sqrt{\omega}} \quad (4-54)$$

here ω is the radial frequency, $j = \sqrt{-1}$, and B is a constant which contains a concentration independent diffusion coefficient.

For a thin film electrode, the diffusion coefficients were obtained by Ho[35]and Wu[112] et al. Here, two extreme cases are considered.

First, if $\omega \gg \frac{2D}{L^2}$, D is the diffusion coefficient and L is the thickness of the thin film electrode. The phase angle is equal to $\pi/4$ [35, 112], thus, Z_w has the form

$$Z_w = |Z| \cos\left(\frac{\pi}{4}\right) - j|Z| \sin\left(\frac{\pi}{4}\right) \quad (4-55)$$

where

$$|Z| = \left| \frac{V_m}{FAD} \frac{dE}{dx} \omega^{-1/2} \right| \quad (4-56)$$

V_m is the molar volume of the materials, A is the electrode's surface area, D is the diffusion coefficient, and $\frac{dE}{dx}$ is the slope of coulometric titration curve.

Comparison of Eq. (4-56) with Eq. (4-54), the diffusion coefficient D can be calculated from the slope of $Z' \sim \frac{1}{\sqrt{\omega}}$ or $Z'' \sim \frac{1}{\sqrt{\omega}}$, B can be written as[35]

$$B = -\frac{V_m}{\sqrt{2FAD}} \frac{dE}{dx} \quad (4-57)$$

The second condition consists in that, if $\omega \ll \frac{2D}{L^2}$, then the phase angle is equal to $\pi/2$. Such phase angle indicates that the current is 90° out of phase with the voltage and is independent of the diffusion coefficient.

Thus, D can be calculated from the limiting low frequency resistance R_L and capacitance C_L . The R_L and C_L can be written as

$$R_L = -\frac{V_m L}{3FAD} \frac{dE}{dx} \quad (4-58)$$

$$\frac{1}{\omega C_L} = -\frac{V_m}{FA\omega L} \frac{dE}{dx} \quad (4-59)$$

From Eq. (4-58) and (4-59), we can get

$$D = \frac{L^2}{3R_L C_L} \quad (4-60)$$

4.5 Phase transformation and intercalation capacitance

At very-low-frequencies, the impedance spectrum starts to deviate from the shape expected due to diffusion alone. The features of EIS of intercalation electrode in the very-low-frequency region are composed of a semicircle and a vertical line, which can be attributed to the phase transformation of the intercalation particles or the growth of a new phase and the

accumulation of lithium ions in the intercalation particles, respectively. These processes could be modeled using a resistance (R_b)-capacitance (C_b) parallel element with a capacitance (C_{int}) in series. Here, R_b and C_b represent the resistance and the capacitance of the phase change of the intercalation particles, C_{int} is the intercalation capacitance of the electrodes.

4.5.1 Phase transformation

Normally, the measured frequency range of EIS in lithium ion batteries system is from 10^5 to 10^{-2} Hz, and the volume changes of the practical intercalation compounds, such as LiCoO_2 , LiMn_2O_4 and graphite materials etc. are not obvious. Moreover, there is little difference between the physical/chemical properties of the two phases which are the new phase and the origin phase. Hence, the semicircle related to the phase transformation is seldom found in EIS in the low-frequency region ($\geq 0.01\text{Hz}$) for the intercalation compounds. However, for the Cu_6Sn_5 [32] alloy or Si anodes for lithium-ion batteries, a new arc is detected which can be attributed to the phase formation process in the low-frequency region (**Figure 4-2**). For the Cu_6Sn_5 alloy, there is a phase transformation process from Cu_6Sn_5 to $\text{Li}_x\text{Cu}_6\text{Sn}_5$ ($0 < x < 13$) under 0.4 V (Li/Li^+) with large volume expansion. Owing to large differences between the physical/chemical properties of the Cu_6Sn_5 phase and that of the $\text{Li}_x\text{Cu}_6\text{Sn}_5$ ($0 < x < 13$) phase, two independent time constants for lithium ions transference in the two phases appear and, as a result, a new arc is formed. For Si anodes, the same phenomenon can be found in the potential region 0.1-0.01 V (Li/Li^+), and there exists a phase transformation process from Si to Li_xSi ($0 < x \leq 4.4$).

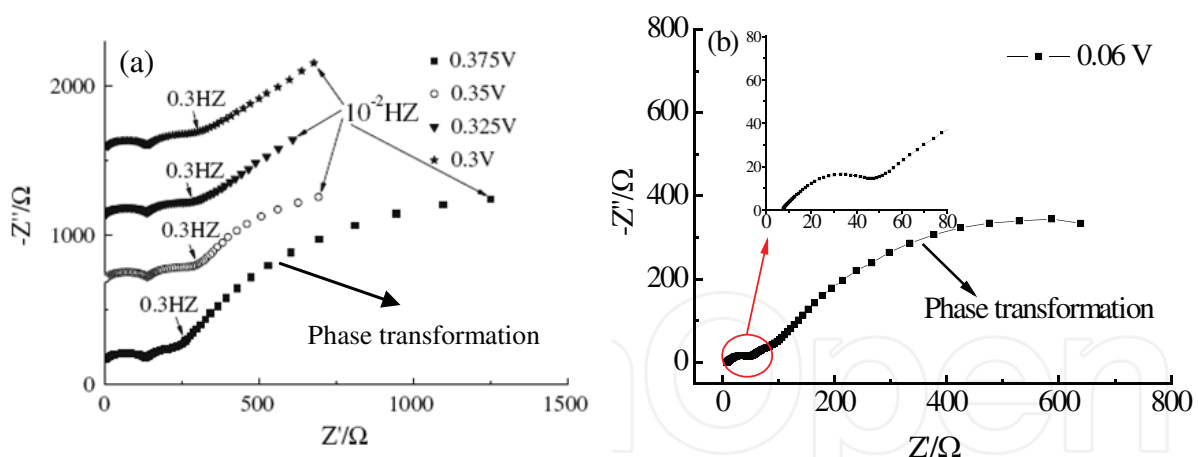


Fig. 4-2. Nyquist plots of Cu_6Sn_5 alloy electrode (a) [32] and Si electrode (b).

4.5.2 Intercalation capacitance

The composition of the intercalation electrode is described in terms of an occupancy fraction $x=n/N$, where n is the number density of intercalated atoms, and N is some number density proportional to the size of the host, such as the number density of one type of site or one type of host atom (i.e. Li in Li_xCoO_2). The steady state voltage of the working electrode, V , is related to the chemical potential of the intercalated atom in the working electrode, μ , and that in the reference electrode, μ_{ref} , by the following equation[64]

$$V = -\frac{1}{e}(\mu - \mu_{ref}) \quad (4-61)$$

where e stands for the positive elementary charge. Note that $z=1$ for Li. The term $-zeV$ is the work done on the cell per ion intercalated under a voltage difference of V . Therefore, the voltage (V) is determined by the variation of the chemical potential of the cathode as a function of composition, $\mu(x)$. Note that measuring the cell voltage at equilibrium versus the charge passed between the electrodes is equivalent to measuring the chemical potential as a function of x , i.e. the Li content of the Li_xCoO_2 compound. The thermodynamics requires that μ increases with the concentration of guest ions, so V decreases as ions are added to the positive electrode. The voltage V is determined by the variation of the chemical potential of the cathode with the composition, $\mu(x)$. The equilibrium intercalation capacitance can be defined in the following way[14]:

$$C_0 = -\frac{dQ}{dV} = LAe^2N \frac{dx}{d\mu} \quad (4-62)$$

where $Q=LANe$ is the total extent of charge passed, L is the film thickness, and A is the area. For noninteracting particles that occupy identical sites of energy E_0 (lattice gas model), the probability of occupancy at equilibrium is determined by Fermi-Dirac statistics

$$F(E_0, \mu) = \frac{1}{1 + \exp[(E_0 - \mu) / k_B T]} \quad (4-63)$$

Generally, one complication of the lattice-gas model applied to intercalation compounds is related to the dissociation of the intercalated atom into ions and electrons. In the present situation, the electronic contributions to the chemical potential (μ) will be neglected so that μ_e (the chemical potential of electrons) is considered as constant, and only μ will be considered to vary as a function of Li insertion, that is, x . Therefore, it is possible to focus attention on the contributions of intercalated ions to the intercalation capacitance. Because $x=n/N = F(E_0, \mu)$, the chemical potential function of ions distributed in the sites of a solid matrix takes the form

$$\mu(x) = E_0 + k_B T \ln\left(\frac{x}{1-x}\right) \quad (4-64)$$

In this case, the intercalation capacitance, C_{int} , is given by:

$$C_0 = \frac{Le^2N}{k_B T} x(1-x) \quad (4-65)$$

At the beginning of lithium ion inserts into or the very end of lithium ion extracts from the active mass during the electrochemical processes, that is to say, for very low insertion level ($x \rightarrow 0$). Eq. (4-65) takes the form

$$C_{int} = \frac{Le^2N}{k_B T} x \quad (4-66)$$

Substituting $x = \exp[f(E - E_0)]$ into Eq. (4-66) and changing the obtained equation to a linear equation by a logarithm, we can obtain the following expression of C_{int}

$$\ln C_{\text{int}} = \ln \frac{Le^2N}{k_B T} + f(E - E_0) \quad (4-67)$$

Eq. (4-67) presents explicitly that, when $x \rightarrow 0$, $\ln C_{\text{int}} \sim E$ shows a linear variation.

A more complete description of intercalation electrodes considers, in addition to the entropic term in Eq. (4-67), other significant effects such as the interactions among ions and the lattice distortions induced by the guest species. In many cases, these effects are described by effective potential terms that are a function of x . An example is the following chemical potential function,

$$\mu(x) = E_0 + k_B T \ln\left(\frac{x}{1-x}\right) + g k_B T x \quad (4-68)$$

where g is the dimensionless interaction parameter that includes both the interactions between intercalated ions and strain fields caused by expansion or contraction of the lattice [45, 96]. The critical value of the interaction parameter is $g = -4$. The capacitance related to Eq. (4-66) is [14, 15]

$$C_{\text{int}} = \frac{Le^2N}{k_B T} \left[g + \frac{1}{x(1-x)} \right]^{-1} \quad (4-69)$$

From the Eq. (4-69), it can be seen that when the insertion lever $x=0.5$, C_{int} has the maximum value. Meanwhile, when $x \rightarrow 0$, that means there are few intercalated lithium ions in the materials' lattice.

C_{int} can be obtained from the imaginary part of the impedance in the limit of very low frequencies, $\omega \rightarrow 0$, thus, C_{int} can be written as the form [46, 51]

$$C_{\text{int}} = -\frac{1}{\omega Z''} \quad (4-70)$$

where ω is the angular frequency of a small-amplitude ac voltage.

5. Impedance spectra of nonhomogeneous, multilayered porous composite intercalation electrode

The electrochemical response of Li insertion electrodes is usually very complicated. In this part, graphite electrodes are discussed as a typical example, since graphite is an excellent electronic conductor, and there is no semicircle related to the electronic properties of graphite materials in the Nyquist plots. The practical ion intercalation electrodes are composite materials, in which the active mass particles are bound to a current collector with PVDF binder, and the electrodes are usually prepared from slurry of the particles and the binder in an organic solvent that spreads out on the current collector, and followed by drying. Therefore, the preparation of composite intercalation electrode coatings, especially

with manual preparation, may result in a nonhomogeneous distribution of the mass of porous electrodes. To analyze the consequence of such a thickness distribution on the electrode's impedance, as shown in **Figure 5-1**, we assume a two-thickness (L_1 and L_2) layer distribution, with a related contribution to the total current of θ_{L1} and $(1-\theta_{L1})$. Every layer composes of only two spherical particles with different radii, r_1 and r_2 . The impedance behavior of the non-homogeneous, multilayered porous composite electrode will be analyzed in the following discussion.

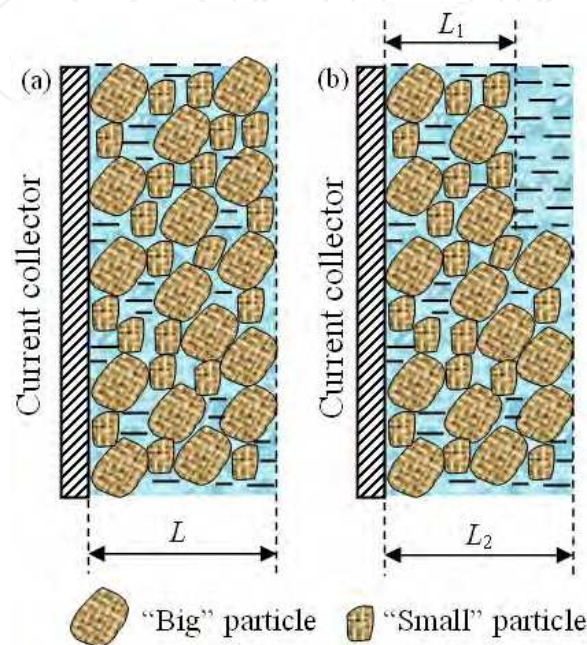


Fig. 5-1. Schematic views of two general models of the porous electrode[115]

Both of the two models of the porous electrode contain two different radii:

(a) homogeneous, porous electrode and (b) nonhomogeneous, multilayered porous electrode.

The total admittance of an electrode which contains two types of spherical particles with different radii ($1/Z_{\text{mix}}$) can be regarded as an averaged sum of the individual admittances $1/Z_{\text{part},1}$ and $1/Z_{\text{part},2}$ [46, 49, 65].

$$\frac{1}{Z_{\text{mix}}} = \frac{\theta_1}{Z_{\text{part},1}} + \frac{1-\theta_1}{Z_{\text{part},2}} \quad (5-1)$$

where θ_1 is the fraction of the total capacity due to a contribution of the "small" particles. $Z_{\text{part},1}$ and $Z_{\text{part},2}$ here represent the impedance of the "small" particles and "big" particles, respectively.

The impedance of an individual insertion/extraction particle can be written from[46]

$$Z_{\text{part},i} = \frac{R_{\text{SEI},i}}{1 + j\omega R_{\text{SEI},i} C_{\text{SEI},i}} + \frac{R_{\text{ct},i} + Z_{\text{W},i}}{1 + j\omega C_{\text{dl},i} [R_{\text{ct},i} + Z_{\text{W},i}]} \quad (5-2)$$

where i denotes particles with different radii, $i=1, 2$; R_{SEI} and C_{SEI} stand for the resistance of ions' migration through the SEI films and the films' capacitance, respectively. Z_{W} is the Warburg resistance, and Z_{W} can be presented in the following form[46]

$$Z_w = \frac{R_{\text{part},i}}{Y_{s,i}} \quad (5-3)$$

with the finite-space diffusion resistive element, $R_{\text{part},i}$ and $(1/Y_{s,i})$ of the form[46, 49, 65]

$$R_{\text{part},i} = \frac{r_{s,i}^2}{3D_s C_{\text{part},i}} = \frac{\tau_i}{3C_{\text{part},i}} \quad (5-4)$$

$$\frac{1}{Y_{s,i}} = \frac{\tanh(\sqrt{j\omega\tau_i})}{(\sqrt{j\omega\tau_i} - \tanh(\sqrt{j\omega\tau_i}))} \quad (5-5)$$

where $C_{\text{part},i}$ is the limiting low-frequency capacitance of a spherical particle, $r_{s,i}$ represents the diameter of the spherical particle, τ_i is the diffusion time constant, and ω is the angular frequency.

Meyers et al.[65] described an important theoretical model for porous intercalation electrodes that consisted of individual spherical particles with different kinds of size distribution (see Fig. 5-1 (a)). For a porous electrode composed of only the same sized spherical particles, the characteristics of EIS are affected by four major parameters, (i) the electronic conductivities of the intercalation particles, ε ; (ii) the solution in the pore space, γ ; (iii) the ratio of the true surface area of the particles to their volume δ ; and (iv) the sharpness of the particles' distribution. The impedance of the porous electrode, Z_{porous} , is relative to the impedance of the mixed particle electrode, and Z_{porous} can be written as the following form[23, 46, 49, 65]

$$Z_{\text{porous}} = \frac{L}{\varepsilon + \gamma} \left[1 + \frac{2 + ((\varepsilon / \gamma) + (\gamma / \varepsilon)) \cosh \nu}{\nu \sinh \nu} \right] \quad (5-6)$$

with the parameter ν of the form

$$\nu = L \left(\frac{\varepsilon + \gamma}{\gamma \varepsilon} \right)^{1/2} \left(\frac{\delta}{Z_{\text{mix}}} \right)^{1/2} \quad (5-7)$$

here, L is the thickness of the porous electrode.

From the Equation (5-1), the impedance of a parallel combination of two porous layers, Z_{L1+L2} , can be expressed below

$$\frac{1}{Z_{L1+L2}} = \frac{\theta_{L1}}{Z_{\text{mix},L1}} + \frac{1 - \theta_{L1}}{Z_{\text{mix},L2}} \quad (5-8)$$

where $Z_{\text{mix},L1}$, $Z_{\text{mix},L2}$ and L_1 , L_2 are the impedance and the thickness of two layers, respectively.

According to the model presented in this study and Eqs. (5-2)-(5-8), a typical Nyquist plot of the electrode that contains three semicircles and a slope line is simulated, which is shown in **Figure 5-2**. As can be seen, the calculated impedance spectroscopy has the similar characteristic with the experimental results, and the impedance plots calculated according to

Eqs. (5-2)-(5-8) are in good qualitative agreement with the experimental impedance spectroscopy of composite, porous graphite electrode. The parameters involved in the calculation are indicated in **Table 5-1** and **5-2**. The calculated thicknesses of the two sublayers are 0.06 and 0.12 cm, which are both thicker than the practical, industrial intercalation electrodes.

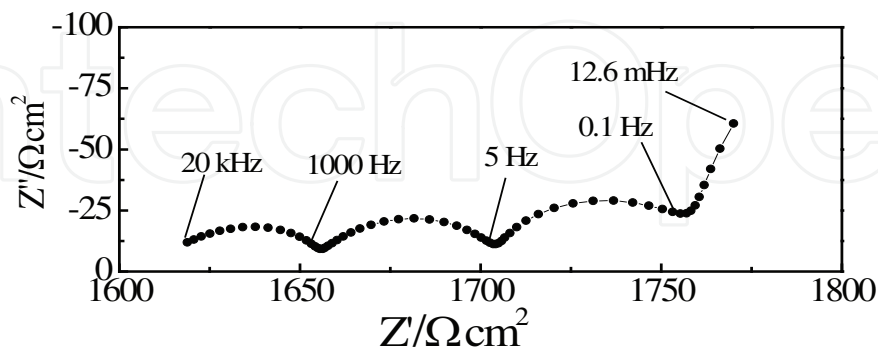


Fig. 5-2. Nyquist plot simulated by computer according to the non-homogeneous, multilayered porous electrode model[115].

	$r_{s,i}/\mu\text{m}$	$R_{\text{part},i}/\Omega\text{ cm}^2$	$C_{\text{dl},i}/\mu\text{F cm}^{-2}$	$R_{\text{ct},i}/\Omega\text{ cm}^2$	$C_{\text{SEL},i}/\mu\text{F cm}^{-2}$	$R_{\text{SEL},i}/\Omega\text{ cm}^2$
Big particles	2	200	200	300	5	100
Small particles	0.3	200	100	200	4	80

Table 5-1. Parameters of the Graphite Particles with Different Radii

Parameters	$D_s/\text{cm}^2\text{ s}^{-1}$	L_1/cm	L_2/cm	δ/cm^{-1}	$\gamma/\Omega^{-1}\text{ cm}^{-1}$	$\varepsilon/\Omega^{-1}\text{ cm}^{-1}$	θ_{L1}	θ_{L2}
Model data	3×10^{-10}	0.06	0.12	5×10^3	5.5×10^{-5}	1×10^{-5}	0.15	0.85

Table 5-2. Porous Structure Parameters

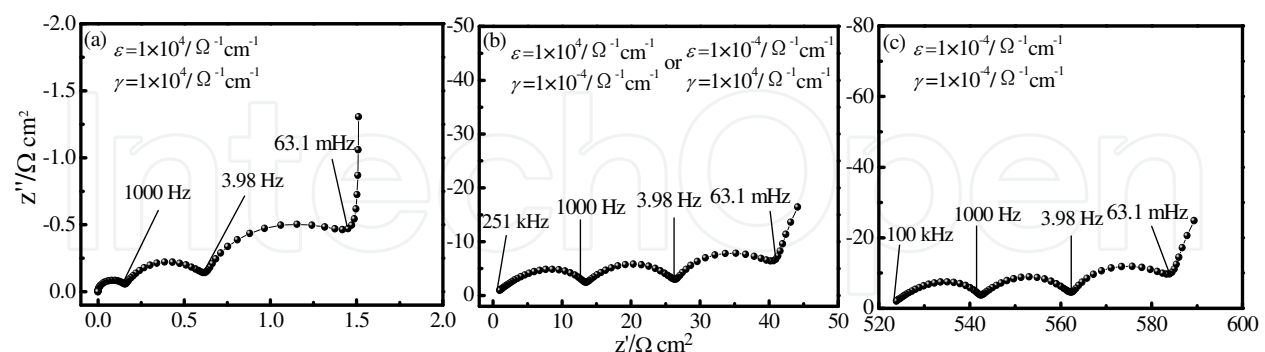


Fig. 5-3. Nyquist plots for a porous electrode composed of mixture of “small” and “big” particles with the different values for ε and γ according to the non-homogeneous, multilayered porous electrode model[115].

To further make clear the limitations and implications of our model, some simulations were carried out to discuss the effect of the porosity of the porous electrode (the electronic conductivities of the insertion particles, ε , and the solution in the pore space, γ), particle size, and the layer distribution on the impedance response of porous electrodes. **Figure 5-3**

illustrates the effect of different ϵ and γ on the impedance structure of a porous electrode composed of mixture of “small” and “big” particles according to the nonhomogeneous, multilayered porous electrode model. Other parameters for the porous electrode are as same as indicated in the **Table 5-1**. It can be seen that, whether the values of the two conductivities are high or low, the feature of the impedance of a porous electrode does not change. When the values of ϵ and γ are increased, it causes a decrease in resistance and capacitance for the whole impedance, together with a drastic shift of the curve along the real impedance axis.

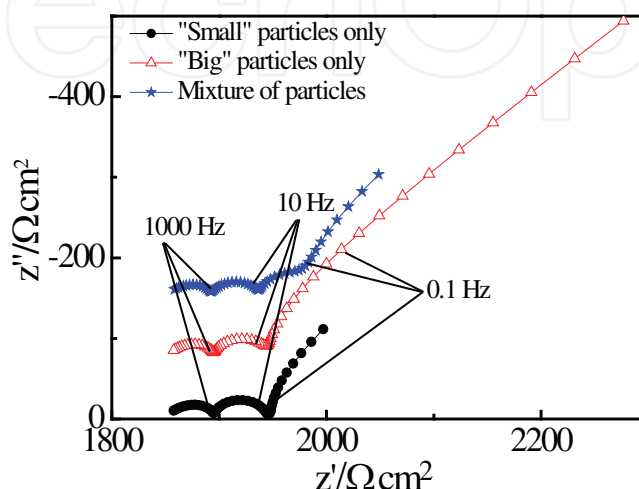


Fig. 5-4. Simulated impedance spectra of a porous electrode composed of “small”, “big” and mixture particles according to the homogeneous, porous electrode model[115].

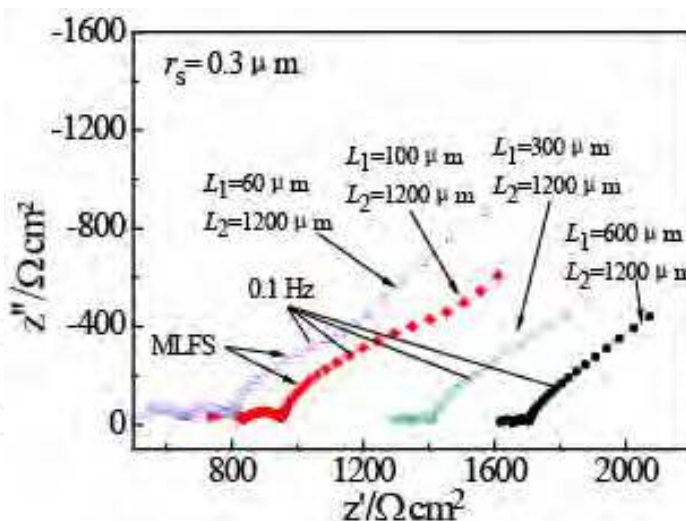


Fig. 5-5. Family of Nyquist plots for a porous electrode composed only of “small” particles with the set of different thickness of the “thinner” layer[115].

The homogeneous, porous electrode model was used to investigate the impedance spectra for a porous electrode composed of “small”, “big”, and mixture of particles. The results are shown in **Figure 5-4**, and the radii of the particles are 0.3 and 1 μm . As can be seen, the shapes of the impedance for the porous electrode with a single particle distribution (“big” or “small” particles) are the same. When the porous electrode contains a mixture of particles,

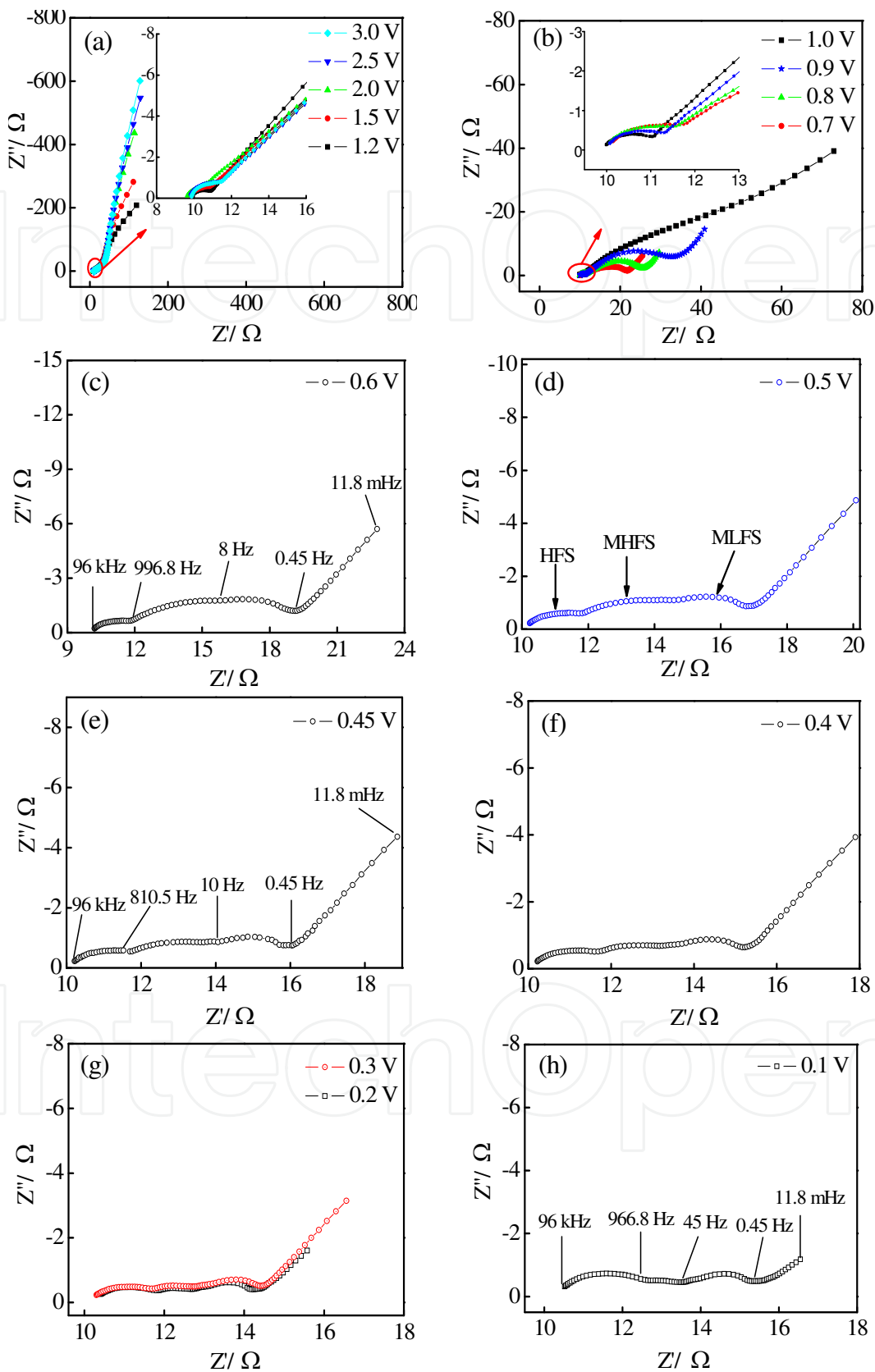


Fig. 5-6. Nyquist plots of the graphite electrode at various potentials from 3.0 to 0.1 V during the first lithium-ion insertion[115].

this yields the impedance spectral feature where an arc is gradually formed in the frequency domain 10-0.1 Hz. This phenomenon demonstrates that the particle size distributions may result in a certain inclination towards an arc in the middle-to-low frequency domain, corresponding to the result reported by Diard et al.[28].

The impedance spectra of a porous electrode composed only of “small” particles with the set of different thickness of the “thinner” layer were obtained in **Figure 5-5**. When the thickness of the “thinner” layer is low, this causes a shift of the curve along the real impedance axis and an arc in the middle-to-low frequency domain is formed gradually.

On the basis of the above analysis, it can be concluded that the particle size and layer distributions may result in a certain inclination toward an arc in the middle-to-low frequency domain. It is worthy to note that an MLFS will be well-developed even if all of the particles have the same radius, but the electrodes are also composed of two parts (thin and thick parts). That is to say, the appearance of the middle-to-low frequency semicircle could be achieved by adopting a nonhomogeneous, layered distribution of the electrode with a different particle size distribution. The nonhomogeneous, multilayered porous electrode model prediction is in good qualitative agreement with the impedance spectra of nonhomogeneous, multilayered porous graphite electrode measured in our previous study[115], as shown in **Figure 5-6**.

6. The inductance formation mechanism

An inductive loop (IL) is often observed in the impedance spectra, but the source for this element in the electrode system remains unclear. An inductance is defined as the properties of an electric circuit that causes an electromotive force to be generated in it as a result of a change in the current flowing through the circuit. Gnanaraj et al.[34] suggested that a plausible explanation for the IL is the formation of an electromotive force superimposed on

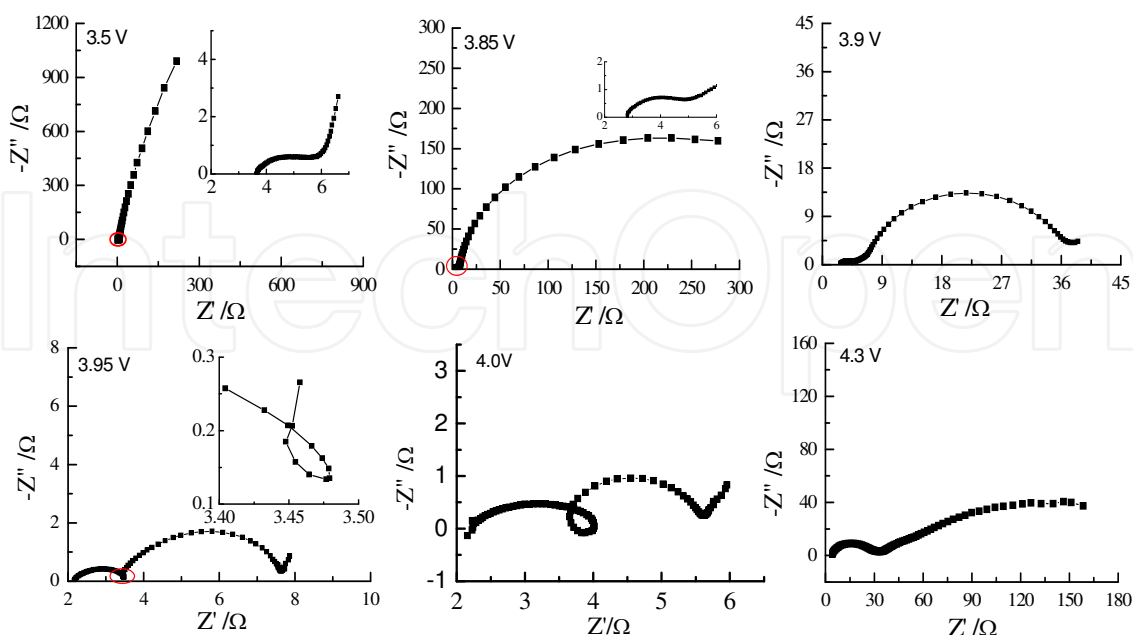


Fig. 6-1. Variations of impedance spectra of LiCoO₂ electrode with the polarization potential in the first delithiation[128].

the lithium ion extraction. The inductive loop has been found in EIS in our previous studies about layered LiCoO_2 [128] and spinel LiMn_2O_4 [127] for lithium ion batteries (see **Figure 6-1**). For layered LiCoO_2 electrode, when lithium ions are extracted from the LiCoO_2 electrode, isolation of Li-rich and Li-poor (deficient) regions in the electrode may be created by the SEI film due to disequilibrium with respect to electronic continuity, thus a concentration cell is established between LiCoO_2 and delithiation LiCoO_2 ($\text{Li}_{1-x}\text{CoO}_2$, $0 < x < 0.5$) separated by the SEI film. Because the SEI film is imperfect in the first delithiation of LiCoO_2 , a current flows within the concentration cell, which generates a field that opposes the field due to the process of lithium ions extraction. The discharge of a concentration cell involves current flow opposed to charging the LiCoO_2 electrode, such a situation meets well with the requirements for the formation of an inductive loop.

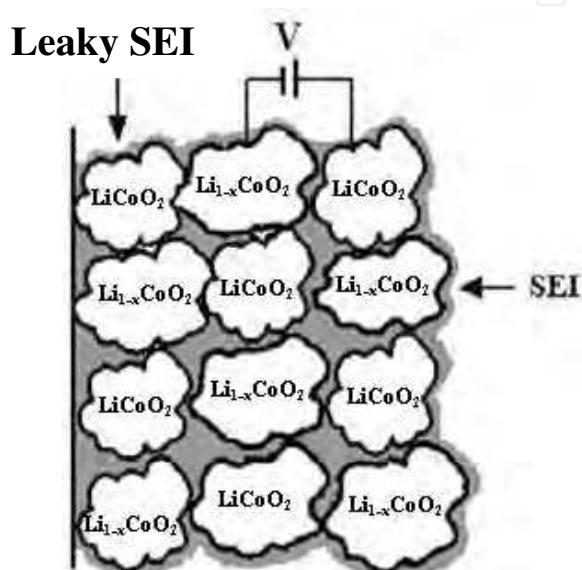


Fig. 6-2. Pictorial representation model for $\text{LiCoO}_2/\text{Li}_{1-x}\text{CoO}_2$ concentration cell[128].

To well understand the inductive loop in the Li/LiCoO_2 cell systems, a pictorial model representation of the SEI film growth and the concentration cell is presented in **Figure 6-2**. With lithium ion extraction from the LiCoO_2 electrode in charge-discharge processed, the $\text{LiCoO}_2/\text{Li}_{1-x}\text{CoO}_2$ concentration cell continues to leak current until the electrode fully deintercalated (corresponding to LiCoO_2 fully converted to $\text{Li}_{0.5}\text{CoO}_2$), i.e. the lithium ion concentration differences in the electrode are removed. Thus, the SEI film on the LiCoO_2 electrode surface may be termed a “leak SEI film”.

For the $\text{Li}/\text{LiMn}_2\text{O}_4$ cell system, an IL also appeared in the potential regions of partial lithium ions deintercalated, that implies the mechanism of the inductance formation is as same as the Li/LiCoO_2 cell system. But interestingly, another IL was turning up along with the former inductive loop at the potential of 3.975 V (see **Figure 6-3**), that means there are two different mechanism of the inductance formation in the $\text{Li}/\text{LiMn}_2\text{O}_4$ cell system, corresponding to two concentration cells exist. When the LiMn_2O_4 fully converted to Mn_2O_4 , the inductive loop was disappeared. As reported in the literature[67, 101], there has a two-step reversible (de)intercalation reaction, in which lithium ions occupy two different tetragonal 8a sites in spinel $\text{Li}_{1-x}\text{Mn}_2\text{O}_4$ ($0 < x < 1$), so the two concentration cells could be signified as $\text{LiMn}_2\text{O}_4/\text{Li}_{1-x}\text{Mn}_2\text{O}_4$ and $\text{Li}_{0.5}\text{Mn}_2\text{O}_4/\text{Li}_{0.5-x}\text{Mn}_2\text{O}_4$ ($0 < x < 0.5$) concentration cells,

and the schematic presentation of models for $\text{LiMn}_2\text{O}_4/\text{Li}_{1-x}\text{Mn}_2\text{O}_4$ and $\text{Li}_{0.5}\text{Mn}_2\text{O}_4/\text{Li}_{0.5-x}\text{Mn}_2\text{O}_4$ ($0 < x < 0.5$) concentration cells is presented in **Figure 6-4**. The IL caused by the $\text{LiMn}_2\text{O}_4/\text{Li}_{1-x}\text{Mn}_2\text{O}_4$ concentration cell appears in the middle-to-high frequency region (~ 100 Hz) in the Nyquist plots, and the middle-to-low frequency region (~ 1 Hz) for $\text{Li}_{0.5}\text{Mn}_2\text{O}_4/\text{Li}_{0.5-x}\text{Mn}_2\text{O}_4$ concentration cell.

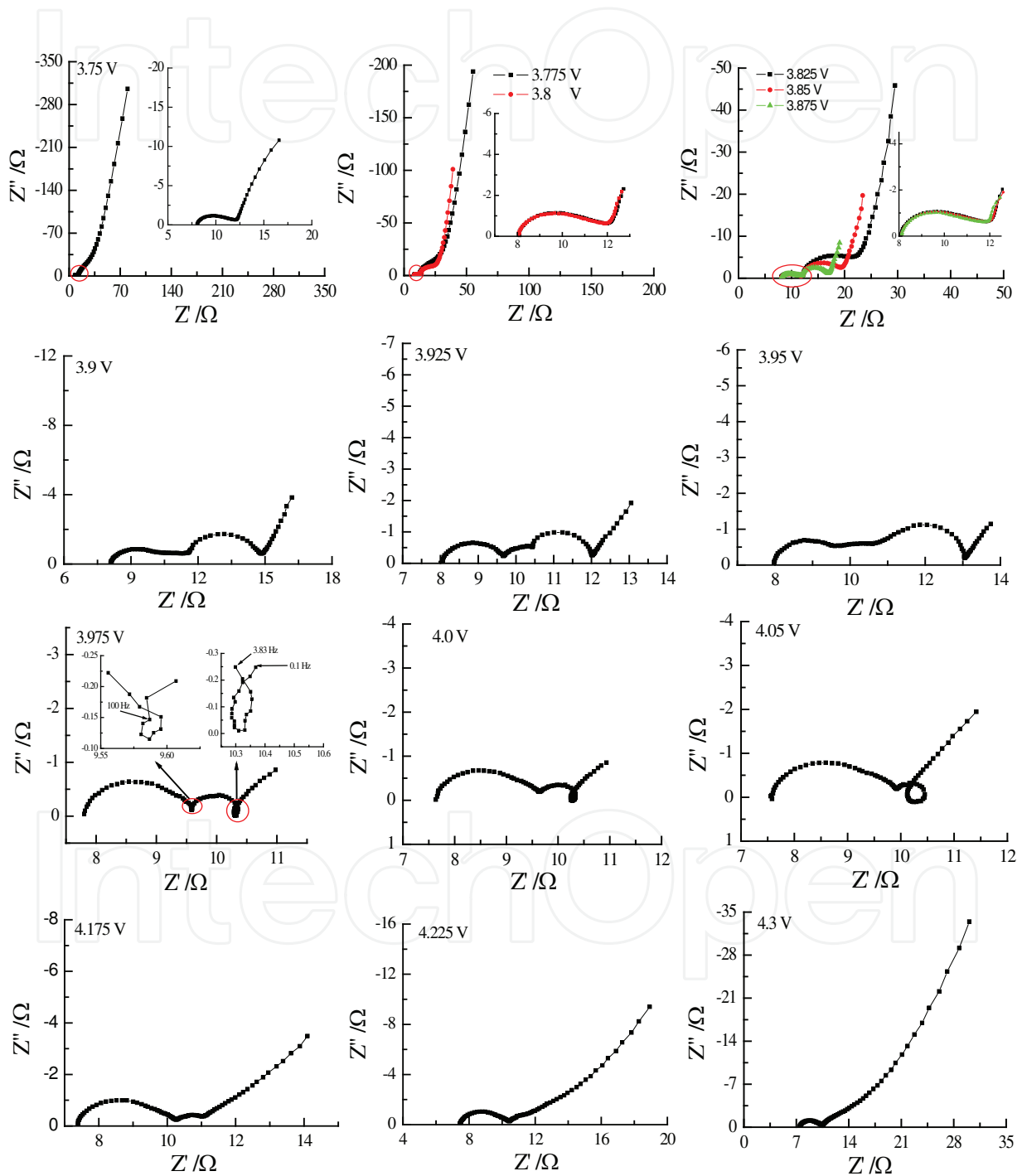


Fig. 6-3. Variations of impedance spectra of LiMn_2O_4 electrode with the polarization potential in the first delithiation[127].

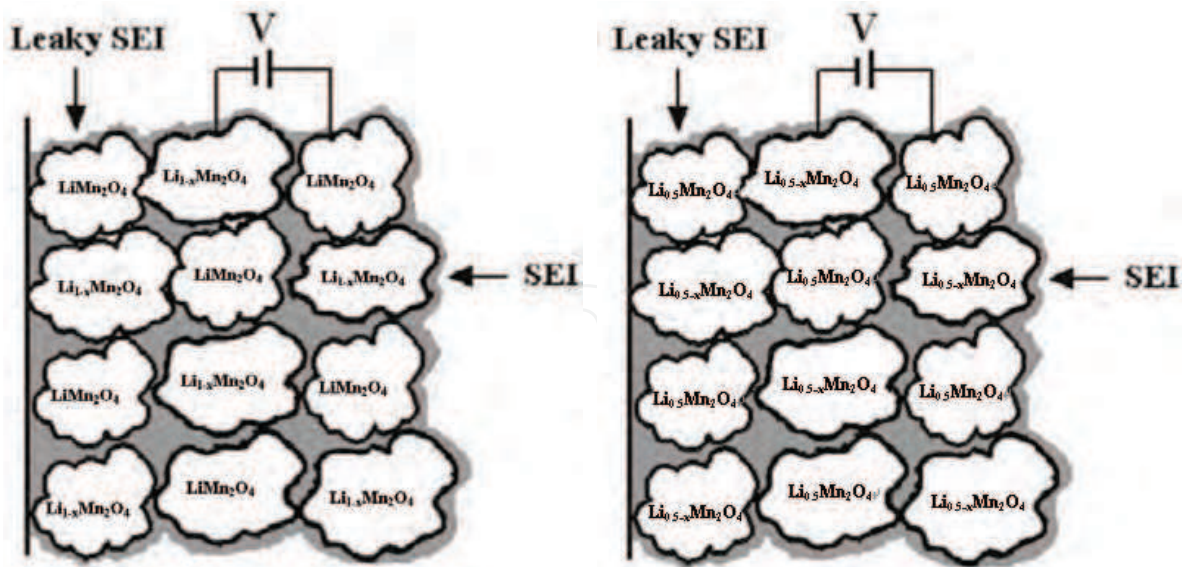


Fig. 6-4. Pictorial representation model for $\text{LiMn}_2\text{O}_4/\text{Li}_{1-x}\text{Mn}_2\text{O}_4$ and $\text{Li}_{0.5}\text{Mn}_2\text{O}_4/\text{Li}_{0.5-x}\text{Mn}_2\text{O}_4$ ($0 < x < 0.5$) concentration cells [127].

7. Conclusions

Impedance measurements have changed the way electrochemists interpret the electrode/electrolyte interface. The technique offers the most powerful analysis on the status of electrodes during charging/discharging processes of lithium-ion batteries. More importantly, this technique may be used to monitor and probe many different processes that occur during electrochemical experiments, including adsorption of reactants and products as well as various reactions that either precede or follow the experiments, thereby changing the electrical characteristics of electrode/electrolyte interfaces. However, there are also some technical matters in application: (i) Lots of factors such as the electrolytic cell system, the composition of intercalation electrode, the content and particle size of active materials, as well as the thickness and preparation of electrode film, can affect the shape and value of the resistance in the impedance spectrum. Therefore, it is important to determine the physical processes corresponding to time constants ranging via theoretical analysis and contrast tests in detail; (ii) A debate is still open on the attribution of time constants relating to different physical processes in lithium insertion, and it needs to be further investigated; (iii) At present, it takes a long time to make impedance measurements in a full frequency region at times more than a few hours, particularly when the frequencies of as low as milli- or submillihertz are included, even for a stable system. Thus, the challenge of the future is to devise the fast impedance technique to shorten its measurement time. At last, correlation of impedance measurements and other experiments (frequently employing non-electrochemical techniques, e.g. in-situ FTIR, in-situ XRD, etc.) would make the analysis of EIS more persuasive.

8. Acknowledgement

This work was supported by the Fundamental Research Funds for the Central Universities (2010LKHX03) and Major State Basic Research Development Program of China (2009CB220102).

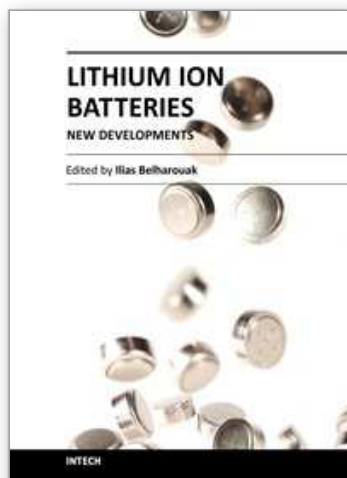
9. References

- [1] Abraham, D. P.; Reynolds, E. M.; Schultz, P. L.; Jansen, A. N.; Dees, D. W. J. *Electrochem. Soc.* 2006, 153, A1610-A1616.
- [2] Atkinson, K. J. W.; Grimes, R. W.; Owens, S. L. *Solid State Ionics* 2002, 150, 443-448.
- [3] Aurbach, D.; Ein-Eli, Y.; Markovsky, B. J. *Electrochem. Soc.* 1995, 142, 2882-2890.
- [4] Aurbach, D.; Gamolsky, K.; Markovsky, B. J. *Electrochem. Soc.* 2000, 147, 1322-1331.
- [5] Aurbach, D.; Levi, M. D.; Levi, E. J. *Electrochem. Soc.* 1998, 145, 3024-3034.
- [6] Aurbach, D.; Zaban, A.; Schechter, A. J. *Electrochem. Soc.* 1995, 142, 2873-2882.
- [7] Badway, F.; Cosandey, F.; Pereira, N.; Amatucci, G. G. J. *Electrochem. Soc.* 2003, 150(10), A1318-A1327.
- [8] Badway, F.; Pereira, N.; Cosandey, F.; Amatucci, G. G. J. *Electrochem. Soc.* 2003, 150(9), A1209-A1218.
- [9] Bard, A. J.; Faulkner, L. R. *Electrochemical Methods Fundamentals and Applications*. John Wiley & Sons, Inc. New York, 2001.
- [10] Barral, G.; Diard, J. P.; Montella, C. *Electrochim. Acta* 1984, 29, 239-246.
- [11] Barsoukov, E.; Kim, D. H.; Lee, H. S.; Lee, H.; Yakovleva, M.; Gao, Y.; Engel, J. F. *Solid State Ionics* 2003, 161, 19-29.
- [12] Barsoukov, E.; Kim, J. H.; Kim, J. H.; Yoon, C. O.; Lee, H. *Solid State Ionics* 1999, 116, 249-261.
- [13] Barsoukov, E.; Macdonald, J. R. *Impedance Spectroscopy Theory, Experiment, and Applications*. John Wiley & Sons, Inc. Hoboken, New Jersey, 2005.
- [14] Bisquert, J. *Electrochim. Acta* 2002, 47, 2435-2449.
- [15] Bisquert, J.; Vikhrenko, V. S. *Electrochim. Acta* 2002, 47, 3977-3988.
- [16] Blomgren, G. E. *J. Power Sources* 1999, 81-82, 112.
- [17] Boukamp, B. A. *Solid State Ionics* 2004, 169, 65-73.
- [18] Brett, C. M. A.; Oliveira, B. A. M. *Electrochemistry, Principles, Methods, and Applications*, Oxford University Press, 1993.
- [19] Bruce, P. G.; Saidi, M. Y. *J. Electrochem. Chem.* 1992, 322, 93-105.
- [20] Bruce, P. G.; Saidi, M. Y. *Solid State Ionics* 1992, 51, 187-190.
- [21] Card, H. C.; Rhoderick, E. H.; *J. Phys. D* 1971, 4, 1589-1601.
- [22] Chang, B. Y.; Park, S. M. *Annu. Rev. Anal. Chem.* 2010, 3, 207-29.
- [23] Chang, Y. C.; Sohn, H. J. *J. Electrochem. Soc.* 2000, 147, 50-58.
- [24] Chiodelli, G.; Lupotto, P. J. *Electrochem. Soc.* 1991, 138(9), 2073-2711.
- [25] Croce, F.; Nobili, F.; Deptula, A.; Lada, W.; Tossici, R.; D'Epifanio, A.; Scrosati, B.; Marassi, R. *Electrochem. Commun.* 1999, 1, 605-608.
- [26] Débart, A.; Dupont, L.; Patrice, R.; Tarascon, J. M. *Solid State Sci.* 2006, 8(6), 640-651.
- [27] Delahay, P. *New Instrumental Methods in Electrochemistry*, Interscience, New York, 1954.
- [28] Diard, J. P.; Le Gorrec, B.; Montella, C. J. *Electroanal. Chem.* 2001, 499, 67-77.
- [29] Doi, T.; Iriyama, Y.; Abe, T.; Ogumi, Z. *Anal. Chem.* 2005, 77, 1696-1700.
- [30] Dokko, K.; Mohamedi, M.; Fujita, Y.; Itoh, T.; Nishizawa, M.; Umeda, M.; Uchida, I. J. *Electrochem. Soc.* 2001, 148, A422-A426.
- [31] Ely, Y. E.; Aurbach, D. *Langmuir* 1992, 8, 1845-1850.
- [32] Fan, X. Y.; Zhuang, Q. C.; Wei, G. Z.; Huang, L.; Dong, Q. F.; Sun, S. G. *J. Appl. Electrochem.* 2009, 39, 1323-1330.
- [33] Gileadi, E. *Electrode Kinetics for Chemists, Engineers, and Material Scientists*, VCH, New York, 1993.

- [34] Gnanaraj, J. S.; Thompson, R. W.; Iaconatti, S. N. *Electrochem. Solid-State Lett.* 2005, 8(2), A128-132.
- [35] Ho, C.; Raistrick, I. D.; Huggins, R. A. *J. Electrochem. Soc.*, 1980, 127, 343-350.
- [36] Holzapfel, M.; Martinet, A.; Alloin, F.; Gorrec, B. L.; Yazami, R.; Montella, C. J. *Electroanal. Chem.* 2003, 546, 41-50.
- [37] Itagaki, M.; Kobari, N.; Yotsuda, S.; Watanabe, K.; Kinoshita, S.; Ue, M. *J. Power Sources* 2005, 148, 78-84.
- [38] Julien, C. M. *Mater. Sci. Eng. R* 2003, 40, 47-102.
- [39] Kanoh, H.; Feng, Q.; Hirotsu, T.; Ooi, K. *J. Electrochem. Soc.* 1996, 143, 2610-2615.
- [40] Kobayashi, S.; Uchimoto, Y. *J. Phys. Chem. B* 2005, 109, 13322-13326.
- [41] Kurzweil, P. AC Impedance Spectroscopy – A Powerful Tool for the Characterization of Materials and Electrochemical Power Sources. In Proceedings: the 14th International Seminar on Double Layer Capacitors, Deerfield Beach, FL., U.S.A., 2004, December 6-8, p1-16.
- [42] Lasia, A. Applications of the Electrochemical Impedance Spectroscopy to Hydrogen Adsorption, Evolution and Absorption into Metals, In: Modern Aspects of Electrochemistry, Conway, B. E.; R. E. White, Edts, Kluwer/Plenum, New York, 2002, vol. 35, p. 1-49.
- [43] Lasia, A. Electrochemical Impedance Spectroscopy and Its Applications. In: Modern Aspects of Electrochemistry, Conway, B. E.; Bockris, J.; White, R. E. Edts., Kluwer Academic/Plenum Publishers, New York, 1999, Vol. 32, p. 143-248.
- [44] Lawless, K. R. *Rep. Prog. Phys.* 1974, 37, 231.
- [45] Levi, M. D.; Aurbach, D. *Electrochim. Acta* 1999, 45, 167-185.
- [46] Levi, M. D.; Aurbach, D. *J. Phys. Chem. B* 2004, 108, 11693-11703.
- [47] Levi, M. D.; Aurbach, D. *J. Phys. Chem. B* 1997, 101, 4630-4640.
- [48] Levi, M. D.; Aurbach, D. *J. Phys. Chem. B* 2005, 109, 2763-2773.
- [49] Levi, M. D.; Aurbach, D. *J. Power Sources* 2005, 146, 727-731.
- [50] Levi, M. D.; Gamolsky, K.; Aurbach, D. *Electrochim. Acta* 2000, 45, 1781-1789.
- [51] Levi, M. D.; Salitra, G.; Markovsky, B.; et al. *J. Electrochem. Soc.* 1999, 146, 1279-1289.
- [52] Levi, M. D.; Wang, C.; Aurbach, D. *J. Electrochem. Soc.* 2004, 151, A781-A790.
- [53] Li, Y.; Wu, H. *Electrochim. Acta* 1989, 34, 157-159.
- [54] Liao, P.; MacDonald, B. L.; Dunlap, R. A.; Dahn, J. R. *Chem. Mater.* 2008, 20, 454-461.
- [55] Macdonald, D. D. *Electrochim. Acta* 2006, 51, 1376-1388.
- [56] Macdonald, D. D. *Transient Techniques in Electrochemistry*, Plenum Press, New York, 1977.
- [57] Macdonald, J. R. *Ann. Biomed. Eng.* 1992, 20, 289-305.
- [58] Macdonald, J. R. *Electrochim. Acta* 1990, 35(10), 1483-1492.
- [59] Macdonald, J. R. *Impedance Spectroscopy Emphasizing Solid Materials and Systems*, Wiley, New York, 1987.
- [60] Macdonald, J. R. *Solid State Ionics* 2005, 176, 1961-1969.
- [61] Marassi, R.; Nobili, F.; Croce, F.; Scrosati, B. *Chem. Mater.* 2001, 13, 1642-1646.
- [62] Marzec, J.; Świerczek, K.; Przewoźnik, J.; Molenda, J.; R Simon, D.; M Kelder, E.; Schoonman, J. *Solid State Ionics* 2002, 146, 225-237.
- [63] Mauvernay, B.; Doublet, M. L.; Monconduit, L. *J. Phys. Chem. Solids* 2006, 67, 1252-1257.
- [64] McKinnon, W. R.; Haering, R. R. in: White R. E.; Bockris J. O. M.; Conway, B. E. (Eds.), *Modern Aspects of Electrochemistry*, vol.15, Plenum Press, New York, 1983, p. 235.

- [65] Meyers, J. P.; Doyle, M.; Darling, R. M.; Newman, J. J. *Electrochem. Soc.* 2000, 147, 2930-2940.
- [66] Mirzaeian, M.; Hall, P. J. *J. Power Sources* 2010, 195, 6817-6824.
- [67] Miura, K.; Yamada, A.; Tanaka, M. *Electrochim. Acta* 1996, 41, 249-256.
- [68] Molenda, J. *Solid State Ionics* 2004, 175, 203.
- [69] Molenda, J. *Solid State Ionics* 2005, 176, 1687.
- [70] Molenda, J.; Swierczek, K.; Kucza, W.; Marzec, J.; Stoklosa, A. *Solid State Ionics* 1999, 123, 155-163.
- [71] Nakayama, M.; Ikuta, H.; Uchimoto, Y.; Wakihara, M.; Kawamura, K. *J. Phys. Chem. B* 2003, 107, 10603-10607.
- [72] Nobili, F.; Dsoke, S.; Corce, F.; Marassi, R. *Electrochimica Acta* 2005, 50, 2307-2313.
- [73] Nobili, F.; Dsoke, S.; Minicucci, M.; Croce, F.; Marassi, R. *J. Phys. Chem. B* 2006, 110 (23), 11310-11313.
- [74] Nobili, F.; Tossici, R.; Croce, F.; Scrosati, B.; Marassi, R. *J. Power Sources* 2001, 94, 238-241.
- [75] Nobili, F.; Tossici, R.; Marassi, R.; Croce, F.; Scrosati, R. *J. Phys. Chem. B* 2002, 106, 3909-3915.
- [76] Okumura, T.; Fukutsuka, T.; Matsumoto, K.; Orikasa, Y.; Arai, H.; Ogumi, Z.; Uchimoto, Y. *J. Phys. Chem. C* 2011, 115(26), 12990-12994.
- [77] Orazem, M. E.; Tribollet, B. *Electrochemical Impedance Spectroscopy*. John Wiley & Sons, Inc. Hoboken, New Jersey, 2008.
- [78] Osaka, T.; Nakade, S.; Rajamäki, M.; Momma, T. *J. Power Sources* 2003, 119-121, 929-933.
- [79] Park, S. M.; Yoo, J. S.; Chang, B. Y.; Ahn, E. S. *Pure Appl. Chem.* 2006, 78(5), 1069-1080.
- [80] Peled, E. *J. Electrochem. Soc.* 1979, 126, 2047-2051.
- [81] Pereira, N.; Dupont, L.; Tarascon, J. M.; Klein, L. C.; Amatucci, G. G. *J. Electrochem. Soc.* 2003, 150(9), A1273-1286.
- [82] Pereira, N.; Klein, L. C.; Amatucci, G. G. *J. Electrochem. Soc.* 2002, 149(3), A262-A271.
- [83] Pistoia, G.; Zane, D.; Zhang, Y. *J. Electrochem. Soc.* 1995, 142(8), 2551-2557.
- [84] Poizot, P.; Laruelle, S.; Grugeon, S.; Dupont, L.; Tarascon, J. M. *Nature* 2000, 407, 496-499.
- [85] Ramadass, P.; Haran, B.; White, R.; Popov, B. N. *J. Power Sources* 2003, 123, 230.
- [86] Rhoderick, E. H.; Williams, R. H. *Metal-Semiconductor Contacts*; Clarendon: Oxford, 1988.
- [87] Rodrigues, S.; Munichandraiah, N.; Shukla, A. K. *J. Power Sources* 2000, 87, 12-20.
- [88] Shi, Y. L.; Shen, M. F.; Xu, S. D.; Qiu, X. Y.; Jiang, L.; Qiang, Y. H.; Zhuang, Q. C.; Sun, S. G. *Int. J. Electrochem. Sci.* 2011, 6, 3399-3415.
- [89] Silva, D. C. C.; Crosnier, O.; Ouvrard, G.; Greedan, J.; Safa-Sefat, A.; Nazar, L. F. *Electrochem. Solid-State Lett.* 2003, 6(8), A162-A165.
- [90] Sluyters-Rehbach, M.; Sluyters, J. H. in E. Yeager, J. O' M. Bockris, B. E. Conway, S. Sarangapini (Eds.), *Comprehensive Treatise of Electrochemistry*, Plenum, New York, 1984, Vol. 9, p. 177.
- [91] Sluyters-Rehbach, M.; Sluyters, J. H. in *Electroanalytical Chemistry*, Bard, A. J. Ed. Marcel Dekker, New York, 1977, Vol. 4, p. 1-127.
- [92] Smith, A. J.; Burns, J. C.; Zhao, X. M.; Xiong, D. J.; Dahn, J. R. *J. Electrochem. Soc.* 2011, 158 (5), A447-A452.
- [93] Song, J. Y.; Lee, H. H.; Wang, Y. Y. et al. *J. Power Sources* 2002, 111, 255-267.
- [94] Souza, D. C. S.; Pralong, V.; Jacobson, A. J.; Nazar, L. F. *Science* 2002, 296(5575), 2012-2015.

- [95] Spontiz, R. J. *Power Sources* 2003, 113, 72.
- [96] Stromme, M. *Phys. Rev. B* 1998, 58, 11015.
- [97] Sun, X. G.; Dai, S. J. *Power Sources* 2010, 195, 4266-4271.
- [98] Sze, S. M. *Physics of Semiconductor Devices*; Wiley: New Jersey, 1981.
- [99] Takamura, T.; Endo, K.; Fu, J.; Wu, Y.; Lee, K. J.; Matsumoto, T. *Electrochim. Acta* 2007, 53, 1055-1061.
- [100] Thackeray, M. M. *Prog. Solid State Chem.* 1997, 25, 1.
- [101] Thackeray, M. M.; David, W. I. F.; Bruce, P. G. et al. *Mater. Res. Bull.* 1983, 18, 461-472.
- [102] Thomas, M. G. S. R.; Bruce, P. G.; Goodenough, J. B. J. *Electrochem. Soc.* 1985, 132, 1521-1528.
- [103] Umeda, M.; Dokko, K.; Fujita, Y.; Mohamedi, M.; Uchida, I.; Selman, J. R. *Electrochim. Acta* 2001, 47, 885-890.
- [104] Van der Ven, A.; Aydinol, M. K.; Ceder, G. *Mater. Res. Soc. Symp. Proc.* 1998, 496, 121.
- [105] Van, E. J.; Wieland, J. L.; Eskes, H.; Kuiper, P.; Sawatzky, G. A.; De Groot, F. M. F.; Turner, T. S.; *Phys. Rev. B* 1992, 44, 6090.
- [106] Verma, P.; Maire, P.; Novák P. *Electrochim. Acta* 2010, 55, 6332-6341.
- [107] Vetter, K. J. *Electrochemical Kinetics*, Academic Press, New York, 1967.
- [108] Wang, Y.; Fu, Z. W.; Yue, X. L. et al. *J. Electrochem. Soc.* 2004, 151(4), E162-E167.
- [109] Wei, T.; Zhuang, Q. C.; Wu, C.; Cui, Y. L.; Fang, L.; Sun, S. G. *Acta Chim. Sinica* 2010, 68, 1481-1486.
- [110] Whittingham, M. S. *Chem. Rev.* 2004, 104, 4271.
- [111] Whittingham, M. S. *Prog. Solid State Chem.* 1978, 12, 41.
- [112] Wu, H. Q.; Li, Y. F. *Electrochemical kinetics*. Beijing: China Higher Education Press, 1998, 217-225.
- [113] Xu, K. *Chem. Rev.* 2004, 104, 4303-4417.
- [114] Xu, K.; Cresce, A. V.; Lee, U. *Langmuir* 2010, 26(13), 11538-11543.
- [115] Xu, S. D.; Zhuang, Q. C.; Tian, L. L.; et al. *J. Phys. Chem. C* 2011, 115, 9210-9219.
- [116] Xue, M. Z.; Fu, Z. W. *Electrochem. Commun.* 2006, 8(12): 1855-1862.
- [117] Yamada, I.; Abe, T.; Iriyama, Y.; Ogumi, Z. *Electrochem. Commun.* 2003, 5, 502-505.
- [118] Yamada, I.; Iriyama, Y.; Abe, T.; Ogumi, Z. *J. Power Sources* 2007, 172, 933-937.
- [119] Yamada, Y.; Iriyama, Y.; Abe, T.; Ogumi, Z. *Langmuir* 2009, 25(21), 12766-12770.
- [120] Yamakawa, N.; Jiang, M.; Grey, C. P. *Chem. Mater.* 2009, 21, 3162-3176.
- [121] Yoo, J. S.; Park, S. M. *Anal. Chem.* 2000, 72, 2035-2041.
- [122] Yoshida, T.; Takahashi, M.; Morikawa, S.; Ihara, C.; Katsukawa, H.; Shiratsuchi, T.; Yamakic, J. J. *Electrochem. Soc.* 2006, 153, A576.
- [123] Yu, F.; Zhang, J. J.; Wang, C. Y. *Progress in Chemistry* 2010, 22(1), 9-18.
- [124] Zaban, A.; Zinigrad, E.; Aurbach, D. *J. Phys. Chem.* 1996, 100, 3089-3101.
- [125] Zhuang, Q. C.; Wei, G. Z.; Xu, J. M.; Fan, X. Y.; Dong, Q. F.; Sun, S. G. *Acta Chimica Sinica*. 2008, 66, 722-728.
- [126] Zhuang, Q. C.; Wei, T.; Du, L. L.; Cui, Y. L.; Fang, L.; Sun, S. G. *J. Phys. Chem. C* 2010, 114, 8614-8621.
- [127] Zhuang, Q. C.; Wei, T.; Wei, G. Z. et al. *Acta Chim. Sinica* 2009, 67(19), 2184-2192.
- [128] Zhuang, Q. C.; Xu, J. M.; Fan, X. Y.; Wei, G. Z.; Dong, Q. F.; Jiang, Y. X.; Huang, L.; Sun, S. G. *Sci. China, Ser. B* 2007, 50(6), 776-783.



Lithium Ion Batteries - New Developments

Edited by Dr. Ilias Belharouak

ISBN 978-953-51-0077-5

Hard cover, 226 pages

Publisher InTech

Published online 24, February, 2012

Published in print edition February, 2012

The eight chapters in this book cover topics on advanced anode and cathode materials, materials design, materials screening, electrode architectures, diagnostics and materials characterization, and electrode/electrolyte interface characterization for lithium batteries. All these topics were carefully chosen to reflect the most recent advances in the science and technology of rechargeable Li-ion batteries, to provide wide readership with a platform of subjects that will help in the understanding of current technologies, and to shed light on areas of deficiency and to energize prospects for future advances.

How to reference

In order to correctly reference this scholarly work, feel free to copy and paste the following:

Quan-Chao Zhuang, Xiang-Yun Qiu, Shou-Dong Xu, Ying-Huai Qiang and Shi-Gang Sun (2012). Diagnosis of Electrochemical Impedance Spectroscopy in Lithium-Ion Batteries, *Lithium Ion Batteries - New Developments*, Dr. Ilias Belharouak (Ed.), ISBN: 978-953-51-0077-5, InTech, Available from:

<http://www.intechopen.com/books/lithium-ion-batteries-new-developments/diagnosis-of-electrochemical-impedance-spectroscopy-in-lithium-ion-batteries>

INTECH

open science | open minds

InTech Europe

University Campus STeP Ri
Slavka Krautzeka 83/A
51000 Rijeka, Croatia
Phone: +385 (51) 770 447
Fax: +385 (51) 686 166
www.intechopen.com

InTech China

Unit 405, Office Block, Hotel Equatorial Shanghai
No.65, Yan An Road (West), Shanghai, 200040, China
中国上海市延安西路65号上海国际贵都大饭店办公楼405单元
Phone: +86-21-62489820
Fax: +86-21-62489821

© 2012 The Author(s). Licensee IntechOpen. This is an open access article distributed under the terms of the [Creative Commons Attribution 3.0 License](#), which permits unrestricted use, distribution, and reproduction in any medium, provided the original work is properly cited.

IntechOpen

IntechOpen